Risk Assessment for Submarine Slope Stability: Numerical Modeling of Flow around a Sliding Soil Mass

By

Stephen G. Wright, Professor, Geotechnical Engineering
University of Texas at Austin

Final Project Report
Prepared for the Minerals Management Service
Under the MMS/OTRC Cooperative Research Agreement
1435-01-99-CA-31003
Task Order 73648
1435-01-04-CA-35515
Task Order 35986
MMS Project Number 491

December 2005

OTRC Library Number: 12/05B159

"The views and conclusions contained in this document are those of the authors and should not be interpreted as representing the opinions or policies of the U.S. Government. Mention of trade names or commercial products does not constitute their endorsement by the U. S. Government".

For more information contact:

Offshore Technology Research Center
Texas A&M University
1200 Mariner Drive
College Station, Texas 77845-3400
(979) 845-6000

or

Offshore Technology Research Center
The University of Texas at Austin
1 University Station C3700
Austin, Texas 78712-0318
(512) 471-6989

A National Science Foundation Graduated Engineering Research Center

TABLE OF CONTENTS

TABLE OF CONTENTS i

LIST OF TABLES AND FIGURES ii

Notation iv

Introduction 1

Assumptions for the Numerical Model 2

Numerical Techniques 3

Development of Numerical Model 4

Case 1 4

Case 2 5

Case 3 6

Case 4 7

Interpretation of Numerical Results for the Flow around a Slide Mass 8

Flow near Bottom 8

Flow near Front 10

Flow near Top 11

Flow near Tail 11

Total Forces on the Soil Mass 12

Lift on Front 12

Conclusions and Discussions 13

Significance 15

References 16

LIST OF TABLES AND FIGURES

Tables

Table 1. Forces applied by the fluid on the sliding mass 12
Table 2: Unit Conversion Chart 46

Figures

Fig. 1 Geometry and co-or system for Case 1 17
Fig. 2 Boundary conditions for Case 1 18
Fig. 3 Mesh for Case 1 19
Fig. 4 Scaled residuals for Case 1 20
Fig. 5 Contours of stream function (kg/s) for Case 1 20
Fig. 6 Geometry for Case 2 21
Fig. 7 Mesh for Case 2 22
Fig. 8 Scaled residuals for Case 2 23
Fig. 9 Contours of stream function (kg/s) for Case 2 23
Fig. 10 Geometry for Case 3 24
Fig. 11 Mesh for Case 3 25
Fig. 12 Scaled residuals for Case 3 26
Fig. 13 Contours of stream function (kg/s) for Case 3 26
Fig. 14 Scaled residuals for Case 4 27
Fig. 15 Horizontal velocity along the right edge for Case 4 27
Fig. 16 Vertical velocity along the right edge for Case 4 28
Fig. 17 The four parts of the surface of the soil mass 29
Fig. 18 Physical & Modeled Flow under Soil Mass 30
Fig. 19 Horizontal velocity across the gap 31
Fig. 20 Vertical velocity across the gap 31
Fig. 20 Vertical velocity across the gap 31
Fig. 21 Kinetic pressure along the bottom of the soil mass 32
Fig. 22 The distribution of shear stress along the bottom of the sliding mass 33
Fig. 23 Pressure distribution around the front of the slide mass 34

Fig. 24 The distribution of the shear stress around the front of the slide mass 35
Fig.25 Pressure distribution along the top surface of the soil mass..... 36
Fig. 26 The distribution of shear stress along the top surface of the soil 37
Fig. 27 The distribution of the kinetic pressure on the tail 38
Fig. 28 The distribution of the shear stress on the tail 39
Fig. 29 Geometry for Case 5..... 40
Fig. 30 Mesh for Case 5 41
Fig. 31 Pressure distribution around the front of the soil mass for Cases 4 and 5..... 42
Fig. 32 Geometry for soil mass for Case 6 43
Fig. 33 Mesh for Case 6..... 44
Fig. 34 Pressure distribution around the front of slide mass for Case 6 45

Notation

Computational fluid dynamics (CFD):

A branch of fluid mechanics where differential mathematical equations such as the Navier-Stokes equations for flow problems are solved numerically using modern digital computers.

Densimetric Froude Number, Fr_d :

Defined as $Fr_d = \dfrac{u}{\sqrt{\left(\dfrac{\rho_d}{\rho_w} - 1\right) gD\cos\theta}}$

where u is the average velocity of sliding, ρ_d and ρ_w are the densities of the soil and water, g is gravity acceleration, D is the average depth of debris and θ is the slope angle of the channel bottom.

FLUENT:

A commercial software package which models fluid flow and heat transfer numerically. Details about the software can be found in the user's documentation for FLUENT 6.1 (FLUENT 6.1 User's Guide, 2005).

GAMBIT:

A software package designed to create models and meshes for computational fluid dynamics (CFD) and other scientific applications.

Kinetic Pressure:

The pressure due to the dynamic effect of the flow. It is also called static pressure in FLUENT.

Lift:

The sum of forces (pressure, viscous, or both) produced by the dynamic action of the flowing fluid that acts normal to the free-stream direction.

Primitive Variables:

Refers to the variables in FLUENT including velocities, mass flow rate of the fluid and Reynolds stresses if involved.

Reynolds Number, Re or Re_x :

In general a non-dimensional index relating to turbulence which usually involves the velocity, characteristic length of the flow and the kinematic viscosity of the fluid.

Specifically, for flow between two plates the Reynolds number Re is defined as $\mathrm{Re} = \frac{uh}{4v}$

where u is the velocity of the inflow, h is the distance between the two plates and v is the kinematic viscosity of the fluid. For flow above a plate, the Reynolds number Re_x is defined as $\mathrm{Re}_x = \frac{ux}{v}$

where u is the reference velocity of the flow, x is the distance from the upstream end of the plate to the location concerned, and v is the kinematic viscosity of the fluid.

Reynolds-Stress Model (RSM):

This is the most elaborate turbulence model that FLUENT provides. It closes the Reynolds-averaged Navier-Stokes equations by solving transport equations for the Reynolds stresses, together with an equation for the dissipation rate.

Scaled Residual, e:

Used/defined in FLUENT as the ratio of the correction to the primitive variable divided by the primitive variable itself for any given iteration. Scaled residuals are calculated for all the primitive variables being solved for in FLUENT. For example, the scaled residual for the horizontal velocity at the $i+1$ iteration is calculated as $e_{Vx}(i+1) = \frac{\left|Vx(i+1) - Vx(i)\right|}{\left|Vx(i+1)\right|}$

where $Vx(i+1)$ is the value of horizontal velocity calculated at the $i+1$ iteration, $Vx(i)$ is the value of horizontal velocity calculated at the i iteration and i is the number of the previous iterations.

Separation:

A phenomenon that the streamlines diverge, the flow separates from the boundary and a recirculation pattern is generated in the region where the boundary turns away from the flow.

Stagnation pressure, $p_{stagnation}$:

Defined as $p_{stagnation} = \frac{1}{2}\rho u^2$

where ρ is the density of water and u is the velocity of the inflow.

Risk Assessment for Submarine Slope Stability: Numerical Modeling of Flow around a Sliding Soil Mass

Introduction

Submarine landslides present an important risk to offshore structures and related facilities such as oil and gas pipelines. Although submarine slides have many similarities to their subaerial counterparts, there are important differences. Hance (2002) conducted a comprehensive survey of submarine slides and developed an extensive database of slope failures. He reported that out of 399 slides examined, 334 occurred on slopes flatter than 10 degrees. He also reported that among a total of 434 slides, 194 slides involved the slide mass traveling a distance of 10 km or more; three slides were reported to have traveled more than 500 km. The reasons for slides on such flat slopes and with such large travel ("run-out") distance are only partially understood. Hydroplaning is one possible mechanism that explains the large run-out distances exhibited by some submarine slides.

This research is focused on the mechanism of slide hydroplaning and developing methodologies that can be used to predict the run-out distances of submarine slides. Such information is necessary for designers to predict the likelihood of a given submarine slide impacting a project site. Once the extent of a slide movement is known, designers will either need to design to resist the soil forces imposed by a slide or avoid the area of impact.

The current research reported on here is focused in particular on the influence of the fluid surrounding a moving slide mass. Previous studies of hydroplaning of submarine slides have employed empirical equations and assumptions to describe the forces exerted by the fluid on the soil mass. This was reported on in the previous progress report for this project. Most of the empirical equations and assumptions have not been verified and in some cases there are contradictions between the theoretical models and experimental observations. For example, Mohrig, et al. (1998) found from model tests that the critical Froude number[1] for hydroplaning is

[1] The Froude number is defined as

$$Fr_d = \frac{u}{\sqrt{\left(\frac{\rho_d}{\rho_w} - 1\right) gD\cos\theta}}$$

0.35. This corresponds to the "lift" [2] produced by the kinetic pressure on the front of the soil mass that is only 4.5 percent of the buoyant weight of soil. Mohrig's observations on when the soil should lift off the underlying material and cause initiation of hydroplaning are not explained by the assumption that the only kinetic pressure on the front of the soil mass is the stagnation pressure at the bottom surface.

In this report, a numerical model is developed to simulate the flow around the sliding soil mass during hydroplaning and to examine the forces applied on the soil mass by the surrounding fluid. In the following sections the basic assumptions made, the numerical modeling techniques employed and the software used for implementation are described. Various cases considered for numerical modeling are presented and the results are described. Finally, important observations and conclusions about the interaction between the fluid and moving soil mass are presented.

Assumptions for the Numerical Model

For the current study the sliding soil mass is treated as a rigid body with a constant velocity. The flow around the sliding soil mass is modeled as two-dimensional, steady flow. The assumptions are reasonable because:

1) For a sliding soil mass with a large width, three-dimensional effects only influence a small region close to the lateral boundaries;
2) For any short interval of time, the deformation and acceleration of the sliding soil mass can be neglected.

For the numerical modeling the length-to-height ratio of the soil mass (L/H), as illustrated in Figure 1 varied from 10 to 20 depending on the particular case and shape of the soil mass. Specific length-to-height ratios are described later for each individual case. The length-to-height ratios used in the numerical modeling are comparable to the ratios used in previous experimental model tests. However the length-to-height ratios of natural slides are often larger than 100. Modeling of length-to-height ratios representative of natural slides presents difficulties in the numerical discretization and solution for several reasons:

1) more than 100 elements along the height of the soil mass are necessary for good modeling of the flow;

---

where u is the average velocity of sliding, ρ_d and ρ_w are the densities of the soil and water, g is gravity acceleration, D is the average depth of debris and θ is the slope angle of the channel bottom.

[2] Lift is the sum of forces (pressure, viscous, or both) produced by the dynamic action of the flowing fluid that acts normal to the free-stream direction.

2) the aspect ratio of elements should be smaller than five;
3) the total number of elements increases as the length-to-height ratio of the soil mass increases;
4) the memory and computational capacities of the available computers limit the total number of elements to less than 1,000,000.

Numerical Techniques

The commercial software FLUENT 6.1 was applied to model the flow numerically. FLUENT is a state-of-the-art computer program for modeling fluid flow and heat transfer with complex geometries. Details about the software can be found in the user's documentation for FLUENT 6.1 (FLUENT 6.1 User's Guide, 2005).

FLUENT is based on a finite volume computational scheme and uses a control-volume-based technique to convert the governing equations for a flow to appropriate linear or nonlinear algebraic equations. The control volume technique involves integrating the governing equations about each control volume, yielding discrete equations that conserve mass on a control-volume basis. Details about the finite volume computational scheme can be found in J. H. Ferziger and M. Peric (2002).

In FLUENT the discrete algebraic equations obtained using the finite volume scheme are solved by numerical iterations. The convergence criterion for the numerical iterations is that all scaled residuals be smaller than 10^{-5}. A scaled residual is defined in FLUENT as the ratio of the correction to the primitive variable divided by the primitive variable itself for any given iteration. Scaled residuals are calculated for all the variables being solved for in FLUENT, including horizontal velocity, vertical velocity, mass flow rate of the fluid and Reynolds stresses if involved. For example, the scaled residual for the horizontal velocity at the $i+1$ iteration is calculated as

$$e_{Vx}(i+1) = \frac{\left|Vx(i+1) - Vx(i)\right|}{\left|Vx(i+1)\right|} \qquad (1)$$

where $Vx(i+1)$ is the value of horizontal velocity calculated in the $i+1$ iteration, $Vx(i)$ is the value of horizontal velocity calculated in the i iteration and i is the number of the previous iterations.

FLUENT incorporates six viscous models for laminar and turbulent flows. The laminar flow model and Reynolds-Stress Model were utilized for the simulations presented in this report. Additional details about viscous models can be found in G. Tzabaris (2000).

FLUENT can solve 2D flow problems with complex geometries using triangular and quadrilateral elements. GAMBIT 2.1 was used as the preprocessor for modeling the geometry and generating meshes. GAMBIT is a software package designed to create models and meshes for computational fluid dynamics (CFD) and other scientific applications. GAMBIT can create 2-D grids consisting of triangular and quadrilateral elements which are supported by FLUENT. The types of elements utilized for the studies presented in this report include rectangles close to the surface of the soil mass and triangles in the rest of the calculation domain. Details about GAMBIT 2.1 can be found in the user's documentation for GAMBIT 2.1 (GAMBIT Modeling Guide, 2004).

Development of Numerical Model

The numerical model was developed through an evolutionary process involving four different cases as described in the following sections. The shape of the soil mass and the flow model varied from case to case. Case 4 was finally selected as the numerical model for the flow around the soil mass.

Case 1

For the first case, the soil mass was represented by a rectangular block as shown in Figure 1. A similar rectangular shape was also used by Harbitz et al. (2003) to model the hydroplaning of subaqueous debris flows analytically. A laminar model was used to simulate the flow. The fluid surrounding the slide mass was considered to be water and the possible shedding of soil into the fluid was neglected.

The coordinate system shown in Figure 1 was assumed to follow the sliding mass. Therefore the soil mass was at rest and the distant fluid and the underlying ground surface were considered to move relative to the coordinate system.

The boundary conditions are illustrated in Figure 2 and are as follows:

1) along the left edge of the calculation domain, a velocity-inlet condition was applied and fluid flowed in through this boundary with a uniform horizontal velocity;

2) at the top edge, a velocity-inlet condition was applied and fluid flowed along this boundary with a uniform horizontal velocity;
3) along the right edge, an outflow boundary condition was applied and flow was assumed to be fully developed and thus did not change along the horizontal direction;
4) the bottom edge was treated as a moving, non-slip wall representing the ground surface moving relative to the soil mass with a constant horizontal velocity;
5) the surfaces of the soil body were stationary non-slip walls since the soil body did not move.

The mesh consists of 601684 rectangular and triangular elements as shown in Figure 3. Rectangular elements are used next to the surfaces of the soil mass and triangular elements are used in the remainder of the calculation domain.

The variation in the scaled residuals with the number of iterations for Case 1 is shown in Figure 4. As shown in Figure 4, the solution never converged. Also shown in Figure 5, the streamlines diverge from the surface of the block near the ends of the block and recirculation patterns develop as indicated by the circled areas. This indicates that separation occurred which results in physical instability of the flow including the development of turbulence and even large eddies. This physical instability prevents the numerical solution from converging.

The occurrence of separation was possibly due to the sharpness of the corners of the block. Near the sharp corners, the streamlines can not turn abruptly to follow the surface of the block. Therefore for the next case the shape of the soil body was modified.

Case 2

For Case 2, the soil mass was represented by a block with rounded corners as shown in Figure 6. The purpose of the rounded corners was to minimize separation of the flow. The rounded corners are also more reasonable because sharp corners are never observed in slides either in the field or laboratory. The coordinate system, flow model and boundary conditions are otherwise the same as for Case 1. The adopted mesh is shown in Figure 7 and the mesh consists of 601684 rectangular and triangular elements.

The variation in the computed residuals with the number of iterations for Case 2 is shown in Figure 8. Again the solution did not converge. As shown in Figure 9 and indicated by the circled

region, separation occurred near the downstream end of the block similar to what occurred in Case 1.

The occurrence of separation was possibly due to the sudden expansion of the flow channel at the downstream end of the block. The streamlines can not abruptly turn to fill the space immediately behind the downstream end of the block. Therefore the shape of the soil mass probably needed to be modified and be more realistic.

Case 3

For Case 3, the soil mass was represented by a streamlined body as shown in Figure 10. This shape was based partly on pictures of slides from Mohrig, et al. (1998)'s experiments and from natural slides reported in the literature and summarized by Hance (2003). The goal of using the streamlined shape was to minimize separation in the flow. The coordinate system, flow model and boundary conditions were otherwise the same as those for Cases 1 and 2. The mesh is shown in Figure 11, and consists of 594812 rectangular and triangular elements.

The variation in the computed residuals with the number of iterations for Case 3 is shown in Figure 12. Once again, the solution did not converge. However as shown by the streamlines in Figure 13, no separation was observed in the flow domain. One possible reason why the solution did not converge is that turbulence developed in the flow domain which could not be modeled by the laminar flow model being used. To examine this further, the flow around the soil mass was compared to the flow along a smooth plate. Crowe, C. T., et.al. (2001) indicated that for flow along a smooth surface the critical value of the Reynolds number Re_x where laminar flow transits into turbulent flow is 5×10^5. The Reynolds number Re_x can be defined as follows:

$$\mathrm{Re}_x = \frac{ux}{v} \qquad (2)$$

where u is the reference velocity of the flow, x is the distance from the upstream end of the plate to the location concerned, and v is the kinematic viscosity of water. The Reynolds number for the flow near the downstream end of the soil mass currently of interest can be calculated as follows

$$\mathrm{Re}_L = \frac{uL}{v} = \frac{1(m/s)\times 20(m)}{10^{-6}(m^2/s)} \approx 10^7 \qquad (3)$$

where L is the length of the soil mass. The Reynolds number 10^7 for the flow near the downstream edge of the soil mass for Case 3 greatly exceeds the critical value 5×10^5. Therefore turbulent flow is likely to develop around the soil mass and the laminar flow model that was assumed is not valid. A turbulent flow model should be used instead.

Case 4

For Case 4, the Reynolds-Stress model was applied to simulate the flow around the soil mass. Since the Reynolds-Stress model simulates turbulent flow only, the flow conditions for Case 4 were first examined to justify the applicability of the Reynolds-Stress model. It was concluded that the flow around the soil mass is turbulent everywhere for the following reasons:

1) as already discussed for Case 3 turbulence develops close to the downstream end of a soil mass;
2) once the head of a sliding mass completely detaches from the main sliding mass, the head becomes an independent soil mass and the flow behind the downstream edge of the head in front of the main body of the slide mass is turbulent;
3) the turbulent flow behind the head becomes the inflow for flow around the main sliding mass i.e. the inflow for flow around the main sliding mass is turbulent;
4) the flow around the main sliding mass is turbulent even in the thin gap between the bottom of the soil mass and the underlying ground surface for the following reasons. Tillmark, N. and P. H. Alfredsson (1992) studied the flow between two parallel plates sliding relative to each other and indicated that the critical value of the Reynolds number Re for the flow to transit from turbulent to laminar is approximately 360. In this case the Reynolds number Re can be defined as follows:

$$\mathrm{Re} = \frac{uh}{4v} \qquad (4)$$

where u is the velocity of the inflow, h is the distance between the two plates and v is the kinematic viscosity of water. The Reynolds number Re for flow between the bottom of the moving soil mass and the underlying ground surface can be calculated by substituting values for Case 4 into Equation 4,

$$\mathrm{Re} = \frac{uh}{4v} = \frac{1(m/s) \times 0.01(m)}{4 \times 10^{-6}(m^2/s)} \approx 10^4 \qquad (5)$$

Thus the Reynolds number Re for the flow between the bottom of the soil mass and the ground surface is much larger than the critical value. The flow should remain turbulent between the bottom of the soil mass and the underlying ground surface.

Based on the above, the flow around the main sliding mass was concluded to be turbulent everywhere.

For Case 4, the coordinate system, shape of the soil mass and boundary conditions are the same as for Case 3. The mesh was also the same as for Case 3. The variation in the computed residuals with the number of iterations for Case 4 is shown in Figure 14. In this case, the solution converged. The distributions of the horizontal and vertical velocities along the right boundary of the flow domain are shown in Figures 15 and 16 respectively. It is seen that the velocities are constant along the vertical direction and are the same as those along the inflow boundary at the left edge of the flow domain. The flow downstream of the right boundary would be uniform and therefore the soil mass only influenced the flow within the domain of calculation, i.e. the extent of the calculation domain is sufficient.

The geometry, Reynolds-Stress flow model and extent of the domain for calculation for Case 4 appear to model the flow around the soil mass realistically. Accordingly the general conditions for Case 4 were selected for subsequent numerical modeling described in the following section.

Interpretation of Numerical Results for the Flow around a Slide Mass

The purpose of modeling flow around a slide mass was to study the forces applied by the fluid on the soil mass, including the pressure and shear along the surface of the soil mass. Based on the analyses for Case 4, the surface of the soil mass can be divided into four parts as shown in Figure 17. Part 1 (AG) is the bottom surface of the soil mass and will be referred to as the Bottom. Part 2 (ABCDE) is the surface of the upstream end of the soil mass and will be referred to as the Front. Part 3 (EF) is the top surface of the central part of the soil mass and will be referred to as the Top. Part 4 (FG) is the upper surface of the downstream end of the soil mass and will be referred to as the Tail. The characteristics of flow and the distributions of pressure and shear stress along the four parts are discussed below.

Flow near Bottom

The bottom surface of the soil mass and the ground surface are parallel to each other and form a gap in Figure 17. The modeling of the flow under the soil mass is soil mass is schematically shown in Figure 18. Three locations (gap-left, gap-middle and gap-right) along the horizontal direction are chosen as shown in Figure 17. The distributions of the horizontal and vertical velocities across the gap at the three locations are shown in

Figures 19 and 20. The velocities are essentially identical at the three locations. This indicates that the flow is uniform within the gap. The vertical velocity is zero. The gradients of horizontal velocity are much greater near the surfaces of the soil mass and the ground.

The distribution of the kinetic pressure[3] along the bottom surface of the soil is shown in Figure 21. The pressure decreases nearly linearly in the horizontal direction from about 350 pa to 120 pa. The gradient of pressure is approximately 13 pa/m.

The distribution of the shear stress along the bottom of the sliding mass is shown in Figure 22. The shear stress is nearly constant. The magnitude of the shear stress is 0.81 pa.

Flow driven by a pressure gradient in a gap with walls moving relative to each other is commonly called "combined Couette-Poiseuille flow", and can be decomposed into Couette flow and Poiseuille flow. The horizontal velocity u of combined laminar Couette-Poiseuille flow can be expressed as follows:

$$u = \frac{1}{2\mu}\frac{dp}{dx}y(y-h) - \frac{u(y=0)}{h}y + u(y=0) \qquad (6)$$

where μ is the dynamic viscosity of water, $\frac{dp}{dx}$ is the gradient of pressure along the x direction, h is the thickness of the gap and $u(y=0)$ is the horizontal velocity at the ground surface. In Equation 6, the first term represents the Poiseuille portion of flow which is driven by pressure. The second and third terms represent the Couette portion of flow which is related to the relative movement of the two walls that form the gap. More details about the combined laminar Couette-Poiseuille flow can be found in Panton., R. L. (1984).

The relative importance of the Poiseuille and Couette portions to the flow near the Bottom can be examined by comparing the first term and the last two terms in Equation 6. Substitute the values of the flow near the Bottom for Case 4 into the first term of Equation 6 yields:

$$\frac{1}{2\mu}\frac{dp}{dx}y(y-h) = \frac{1}{2\times 10^{-3}(pa\cdot s)}\times\left(-13(pa/m)\right)\times y\left(y-0.01(m)\right) \qquad 0 \le y \le 0.01(m)$$

[3] The kinetic pressure is the pressure due to the dynamic effect of the flow. It is also called static pressure in FLUENT 6.0.

The maximum value of the first term in Equation 6 can be calculated as

$$\left.\frac{1}{2\mu}\frac{dp}{dx}y(y-h)\right|_{\max} = \frac{1}{2\times10^{-3}(pa\cdot s)}\times(-13(pa/m))\times0.005(m)(0.005(m)-0.01(m)) = 0.16 \quad (m/s) \quad (7)$$

The maximum value of the last two terms in Equation 6 is $u(y=0)$, which is 1.00 m/s. The first term is much smaller than the last two terms. Therefore the Poiseuille portion of the flow near Bottom can be neglected according to the theory of combined laminar Couette-Poiseuille flow. For the turbulent flow near Bottom, the Couette portion should still be the dominating component. Therefore flow near the Bottom is primarily a turbulent Couette flow. More details about turbulent Couette flows can be found in Egolf, P. W and Weiss, D. A. (1995). The mean velocity profile of a turbulent Couette flow indicated by Egolf, P. W and Weiss, D. A. (1995) is similar to the distribution of the horizontal velocity across the gap shown in Figure 19.

Flow near Front

The distributions of the kinetic pressure and shear stress on the surface of the leading end of the soil mass are shown in Figures 23 and 24 respectively. In Figures 23 and 24, the x-coordinate is the distance along the curved surface ABCDE. The origin corresponds to point C which is the leading point of the slide mass. The positive direction is toward E and the negative direction is toward A. As shown in Figure 23, the maximum magnitudes of the positive and negative pressures are comparable to the stagnation pressure. The stagnation pressure of the flow is defined as

$$p_{stagnation} = \frac{1}{2}\rho u^2 \qquad (8)$$

where ρ is the density of water and u is the velocity of the inflow. The stagnation pressure for the flow around the soil is calculated as

$$p_{stagnation} = \frac{1}{2}\rho u^2 = \frac{1}{2}\times1000(kg/m^3)\times(1.0(m/s))^2 = 500 \quad pa \qquad (9)$$

By numerically integrating the vertical component of the pressures along the surface of Front, the vertical component of the total force due to pressure was calculated to be approximately 2677 newton/m. Also by numerically integrating the vertical component of the shear stress along the surface of Front, the vertical component of the total force due to shear stress was calculated to be 2 newton/m. The sum of the forces in the vertical direction due to pressures and shears is an upward force representing "lift". Since the contribution of shear stress is much smaller than that from the pressure, only the contribution of pressure is considered when the lift is studied later in this report. The lift on the front may change when the thickness of the gap between the bottom of

the soil mass and the ground surface changes and when the frontal shape of the soil mass changes. The influence on the lift by the thickness of the gap between the bottom of the soil mass and the ground surface and the frontal shape of the soil mass is studied in another section.

Flow near Top

The distribution of kinetic pressure along the top surface of the soil mass is shown in Figure 25. The variation in the pressure along the top surface is small and thus the pressure can be considered nearly constant along the top surface. The pressure is about -150 pa.

The distribution of the shear stress along the top surface of the soil mass is shown in Figure 26. The shear stress was also calculated from the theory for a turbulent boundary layer along a flat plate. The shear stress along the surface of a flat plate can be calculated as

$$\tau_x = \frac{1}{2}\rho u^2 \left(\frac{0.027}{\left(\frac{ux}{\upsilon} \right)^{1/7}} \right) \qquad (10)$$

where x is the distance from the upstream end of the plate to the location of concern , τ_x is the shear stress at location x, ρ is the density of water, u is the velocity of the inflow, and υ is the kinematic viscosity of water. Further details on the turbulent boundary layer theory for flow along a flat plate can be found in Crowe, C. T. et. al. (2000). The shear stress calculated using Equation (10) is also shown in Figure 26. It can be seen that the shear stresses calculated from the theory are close to those from the numerical model. Therefore it appears that the shear stress along the top surface of the soil mass can be approximated by the theory for a turbulent boundary layer.

Flow near Tail

The distribution of the kinetic pressure along the upper surface of the Tail is shown in Figure 27. The corresponding distribution of the shear stress along the Tail is shown in Figure 28. It appears that the variation in kinetic pressure and shear stress can be approximated as a linear variation, although there is some deviation from this near the ends of the Tail. The values of pressure and shear stress at the two ends of Tail are the same as those at the downstream ends of Top and Bottom.

Total Forces on the Soil Mass

The total forces applied by the surrounding fluid on the slide mass were calculated by integrating the pressure and shear stress along the surface of the slide mass. The results are shown in Table 1. In the horizontal direction, the contributions to total force are from shear stress on the top and bottom surfaces and pressure on the front and tail surfaces of the soil mass. When the length-to-height ratio of soil mass increases, the contribution of pressure decreases while that of shear stress increases. For slide masses with a length-to-height ratio larger than 20 which is close to Case 4, the contribution to horizontal force from shear stress is more than 85 percent.

In the vertical direction, the contributions to total force are from shear stress on the front and tail surfaces and pressure on the top and bottom surfaces of the soil mass. When the length-to-height ratio of soil mass increases, the contribution of pressure increases while that of shear stress decreases. Because the length-to-height ratio is usually larger than one for slide mass, the major contribution to vertical force is from pressure.

Table 1. Forces applied by the fluid on the sliding mass

	Due to Kinetic pressure	Due to shear stress	Total
Horizontal Force (newton/m)	9.0	50.0	59.0
Vertical Force (newton/m)	8839.8	1.5	8841.3

Lift on Front

In order to study the influence of the gap between the bottom of the soil mass and the ground surface and the frontal shape of the soil mass on the lift applied on the front of the soil mass by the surrounding fluid, two additional cases were analyzed and the results were compared with the results for Case 4.

For Case 5, the thickness of the gap between the bottom of the soil mass and the ground surface was zero. In another word, the soil mass was in contact with the ground surface. The geometry of Case 5 is shown in Figure 29. The boundary conditions are the same as those for Case 4 along the left, top and right edge of the calculation domain. The bottom edge of the calculation domain was a stationary non-slip wall which represented the exposed surfaces of the soil mass and the surfaces of the ground beyond the soil mass. The mesh for Case 5 is shown in Figure 30 and has 553664 rectangular and triangular elements. The coordinate system and flow model for Case 5 are the same as for Case 4.

The front of the soil mass in Case 5 is represented by the surface B'C'D'E' shown in Figure 29. This surface is comparable to the surface BCDE of the soil mass for Case 4 shown previously in Figure 17. The distributions of kinetic pressure along parts BCDE and B'C'D'E' for Cases 4 and 5 are shown together in Figure 31. In Figure 31, the x-coordinate is measured along the curve surfaces BCDE and B'C'D'E' with the origin at points C and C'. As shown in Figure 31 the two pressure distributions are similar. Therefore the presence of a water-filled gap between the moving soil mass and underlying ground has only a small influence on the pressure on the front. Since the lift on the front is mainly due to the pressure, the water-filled gap has little influence on the lift.

For Case 6, the front of the soil mass had a more abrupt curvature than for Case 5. The geometry for Case 6 is shown in Figure 32. The surfaces C'D' and C"D" in Figures 29 and 32 are both of an elliptical shape. The depth-to-width ratios (d/w) for surfaces C'D' and C"D" are respectively 0.4 and 2.0. All the other conditions including coordinate system, boundary conditions and flow model for Case 6 are the same as for Case 5. The mesh for Case 6 is shown in Figure 33 and includes 526722 rectangular and triangular elements.

The front of the soil mass, part C"D"E" is shown in Figure 32. The distribution of kinetic pressure along part C"D"E" is shown in Figure 34. The magnitude of the negative pressure in Figure 34 is much larger than that in Figure 31 for Cases 4 and 5. In all Cases 4, 5 and 6, the negative pressure is applied along the upper side of the fronts CDE, C'D'E' and C"D"E". The increase of the magnitude of the negative pressure for Case 6 increases the lift on the front. Therefore the lift on the front of the soil mass increases when the depth-to-width ratio (d/w) of the front of the soil mass increases.

Conclusions and Discussions

A numerical model has been developed and used to study the flow of water around a moving soil mass. This has produced a better understanding of the flow around a slide mass especially the resulting pressures and shear stresses exerted on the slide mass. The following specific conclusions can be drawn from the numerical modeling:

1) The contribution to the horizontal force from the shear stress at the top and bottom surfaces of the slide mass increases when the length-to-height ratio (L/H) of the mass increases while the contribution from the pressure at the front and tail surfaces decreases;

2) For slide masses with a length-to-height ratio larger than 20, the contribution to the horizontal force from the shear stress is more than 85 percent.
3) The flow in the gap between the bottom of the moving soil mass and underlying ground surface can be described as a turbulent Couette flow;
4) The shear stress along the bottom of the soil mass is constant;
5) The shear stress along the top surface of the slide mass can be estimated using turbulent boundary layer theory for flow over a flat plate;
6) The contribution to the vertical force from the shear stress at the front and tail surfaces of the slide mass decreases when the length-to-height ratio (L/H) of the mass increases while the contribution from the pressure at the top and bottom surfaces increases;
7) For slide masses with a length-to-height ratio larger than 1.0, the contribution to the vertical force from the shear stress is negligible.
8) The kinetic pressure on the bottom surface of the slide mass decreases linearly from the upstream end to the downstream end of the slide mass;
9) The kinetic pressure on the top of the slide mass is nearly constant;
10) The kinetic pressure on the surface of the front of the soil mass is not influenced by the presence of a water-filled gap between the bottom of the soil mass and the ground surface. However the kinetic pressure is influenced by the shape of the front of the soil mass. When the depth-to-width ratio (d/w) of the front increases, the magnitude of the negative kinetic pressure on the front and the total lift increase.

The geometry of the soil masses used for the numerical models is comparable to those used in the laboratory experiments of submarine slides and hydroplaning. Thus the numerical results and conclusions can be applied to the experimental studies directly.

For actual slides offshore, the major difference from the laboratory studies is that the length-to-height ratio (L/H) of the slide mass is larger. The increase of the length-to-height ratio (L/H) will not influence the general conclusions drawn above about the stresses applied by the surrounding fluid on the soil mass due to the following reasons:

1) the flow around the front of the soil mass is not influenced by the length-to-height ratio (L/H) of the slide mass;
2) the kinetic pressure along the top surface of the soil mass is constant and thus not influence by the length-to-height ratio (L/H) of the soil mass;

3) the theory of the turbulent boundary layer on a flat plate considers the change of the shear stress along the top surface of the soil mass and thus is still applicable when the length-to-height ratio (L/H) increases;
4) the flow in the gap between the bottom of the soil mass and the ground surface does not change along the horizontal direction because it is confined by the bottom of the soil mass and the ground surface. The flow in the gap is thus not influenced by the increase of the length-to-height ratio (L/H) of the soil mass;
5) along the bottom of the soil mass, the kinetic pressure still changes linearly and the shear stress remains constant when the length-to-height ratio (L/H) of the soil mass increases.

Significance

For the whole soil mass to hydroplane, the total upward vertical force applied by the surrounding fluid needs to be equal to the downward force due to the buoyant weight of the soil mass. Assuming the underlying ground surface is horizontal for simplicity, the total downward force due to the buoyant weight of a soil mass, G', with unit width (normal to the direction of sliding) can be approximated by Equation (11) as follows:

$$G' = (\rho_d - \rho_w) g\left[(L-t)H + 0.5tH\right] \qquad (11)$$

Where ρ_d and ρ_w are densities of soil and water, g is the acceleration due to gravity. Also as shown in Figure 10, L is the total length of the soil mass, H is the thickness of the soil mass and t is the length of the tail portion of the soil mass. Substituting numbers into Equation 11 using the geometry of the soil mass for Case 4 and the downward force G' is calculated as follows:

$$\begin{aligned} G' &= (2000kg/m^3 - 1000kg/m^3) \times 10 Newton/kg \times \left[(22m - 10m) \times 1m + 0.5 \times 10m \times 1m\right] \\ &= 1.7 \times 10^5 \, Newton/m \end{aligned} \qquad (12)$$

As shown in Table 1, the total upward force applied by the surrounding water is 8841 Newton/m for Case 4. Therefore when the sliding velocity of the soil mass is 1.0 m/s, the whole soil mass for Case 4 does not hydroplane.

Additional study shows that the hydrodynamic stresses are proportional to the stagnation pressure $p_{stagnation}$ as defined in Equation (8). In another word, the hydrodynamic stresses are proportional to the square of the sliding velocity of the soil mass. For example, when the sliding velocity of the soil mass of Case 4 increases to 4.4 m/s, the total upward force due to hydrodynamic stresses will be 1.7E5 Newton/m. Therefore, the whole soil mass for Case 4 will hydroplane when the sliding velocity of the soil mass is about 4.4 m/s.

References

1. Crowe, C. T., Roberson, J. A.,and Elger, D. F. 2000. Engineering Fluid Mechanics. John Wiley and Sons, Inc. New York.
2. De Blasio, F. V., Engvik, L., Harbitz, C. B. and Elverhøi, A., (2004),"Hydroplaning and submarine debris flows," Journal of geophysical research, Vol. 109, C01002, doi: 10.1029/2002JC001714.
3. Egolf, P.W. and Weiss, D. A. 1995. "Model for Plane Turbulent Couette Flow." Physical Review Letters. 75. pp2956-2959.
4. Ferziger, J. H., Peric, M. 2002. Computational Methods for Fluid Dynamics. Springer-Verlag Berlin Heidelberg, New York.
5. Fluent 6.2 User's Guide. 2005. Fluent Inc.
6. Gambit 2.2 Modeling Guide. 2004. Fluent Inc.
7. Hance, J. J., (2002), Development of a database and assessment of seafloor slope stability based on published literature, M.S. thesis, the university of Texas at Austin.
8. Harbitz, C.B., Parker, G., ElverhΦi, A., Marr, J.G., Mohrig, D., and Harff, P.A., 2003, "Hydroplaning of subaqueous debris flows and glide blocks: Analytical solutions and discussion," J. Geophys. Res., 108(B7), 2349, doi:10. 1029/2001 JB001454.
9. Mohrig, D., Ehipple, K. X., Hondzo, M. Ellis, C. and Parker, G, 1998, Hydroplaning of subaqueous debris flows, Geol. Soc. Am.Bull., 110, pp 387-394.
10. Panton, R. L. 1984. Incompressible Flow. John Wiley and Sons, Inc. New York.
11. Tzabaris, G. 2000. Calculation of Complex Turbulent Flows. Southampton, Boston, WIT.

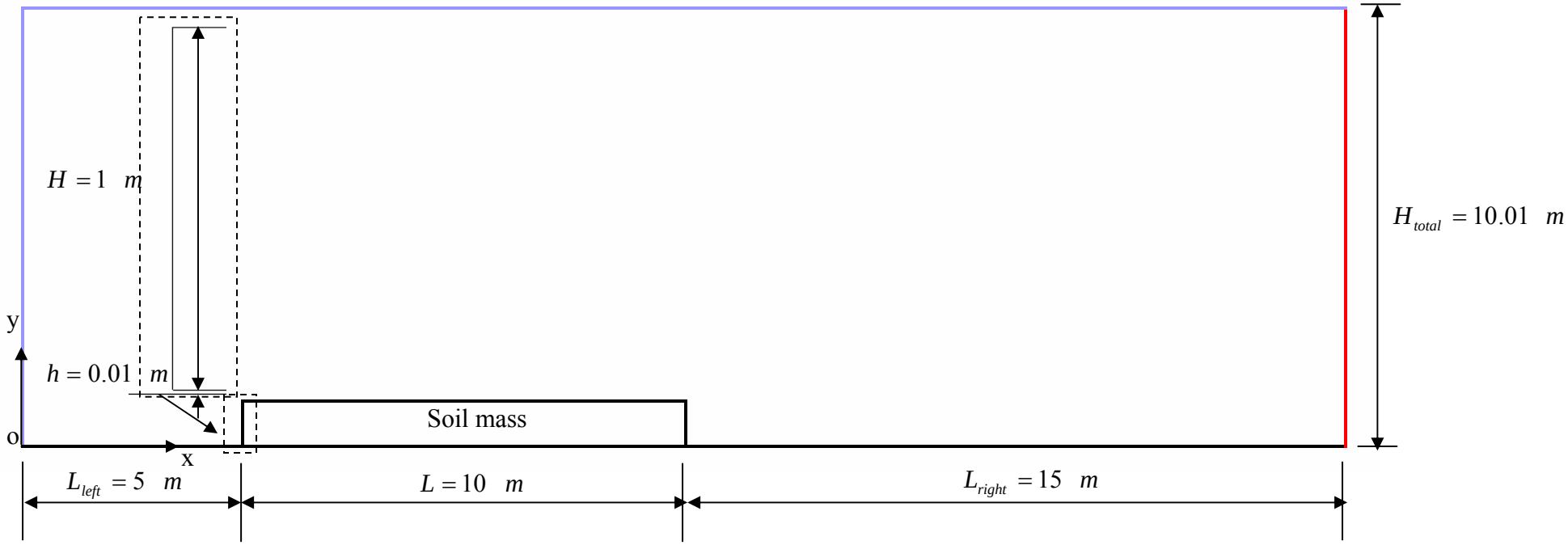

Fig. 1 Geometry and co-or system for Case 1

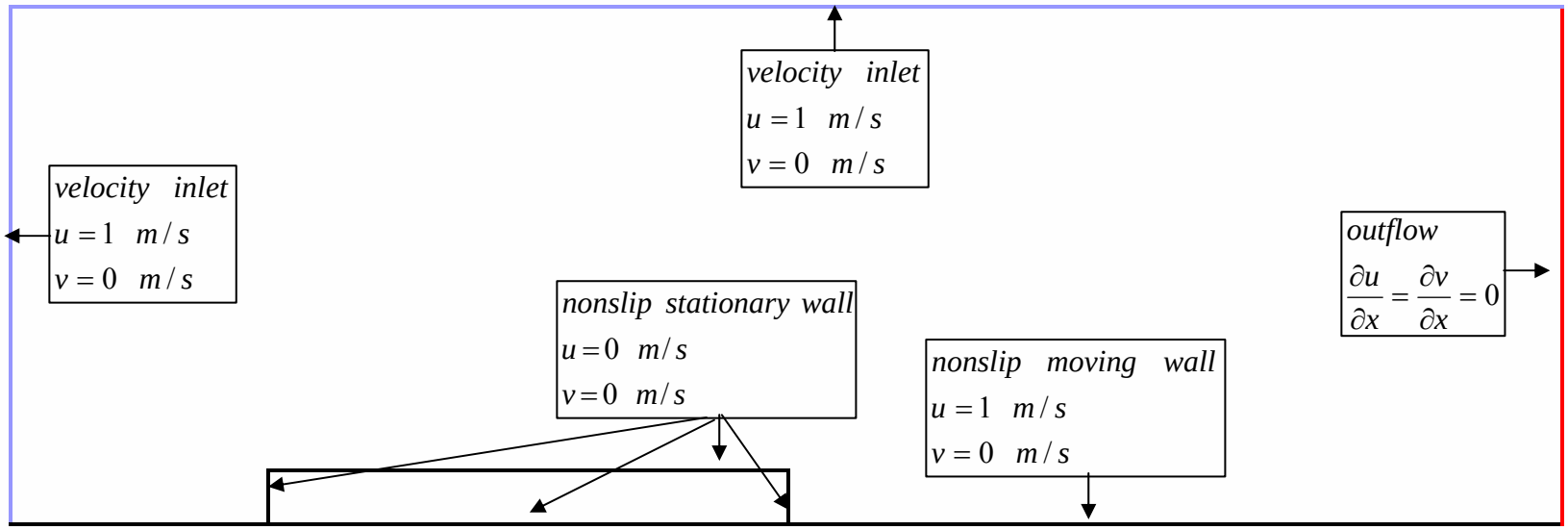

Fig. 2 Boundary conditions for Case 1

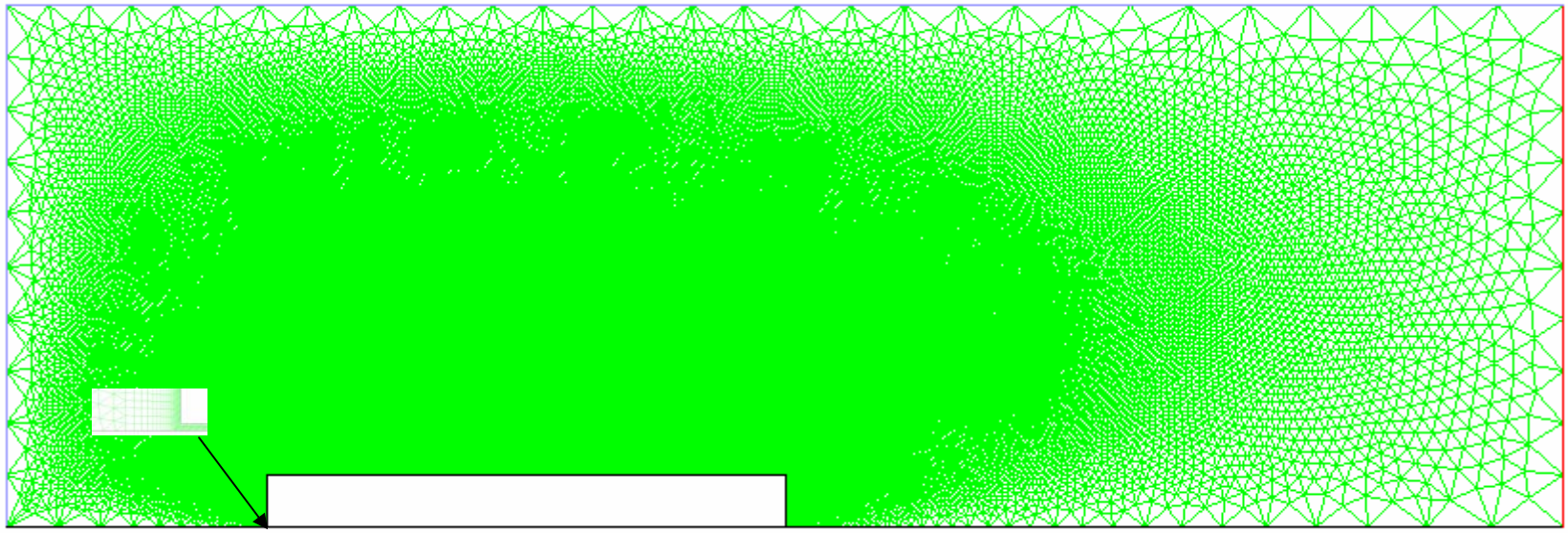

Fig. 3 Mesh for Case 1

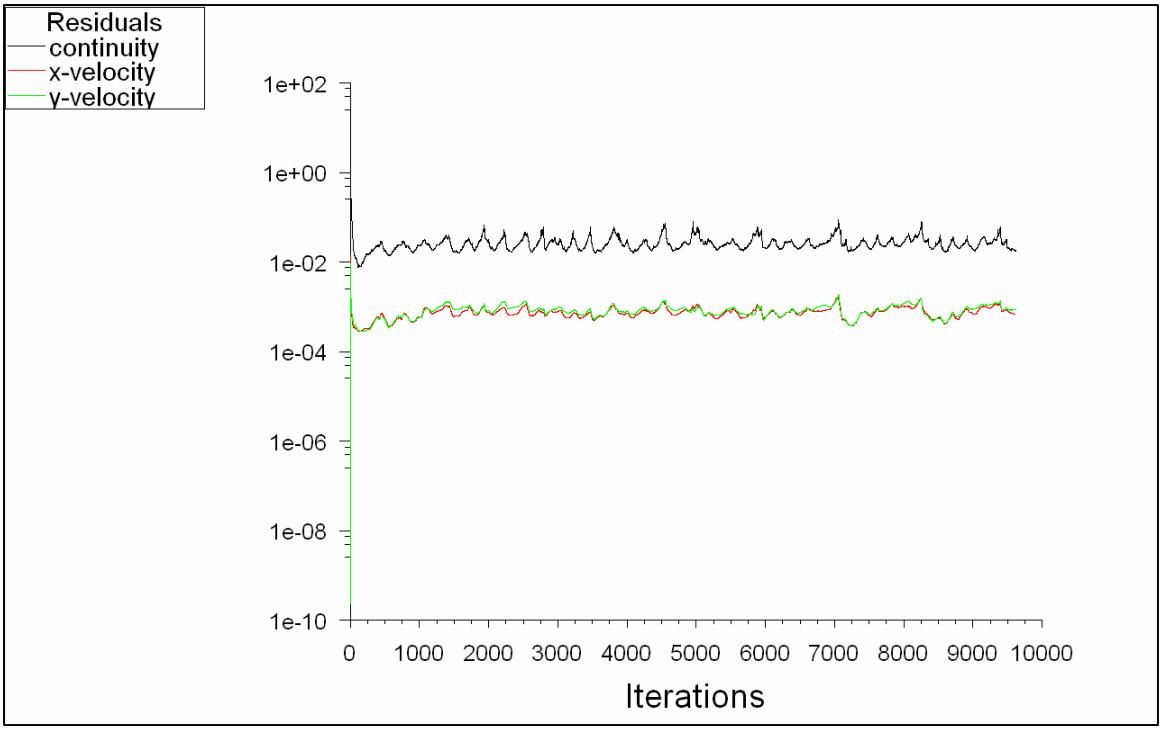

Fig. 4 Scaled residuals for Case 1

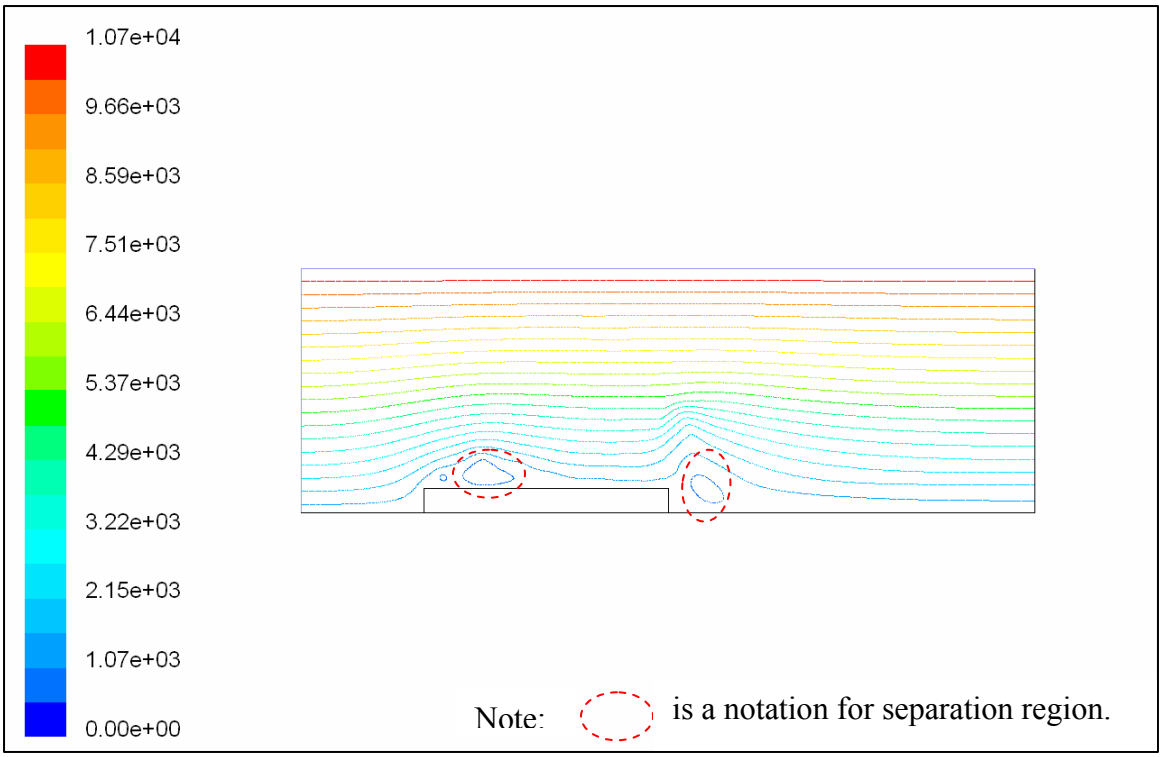

Fig. 5 Contours of stream function (kg/s) for Case 1

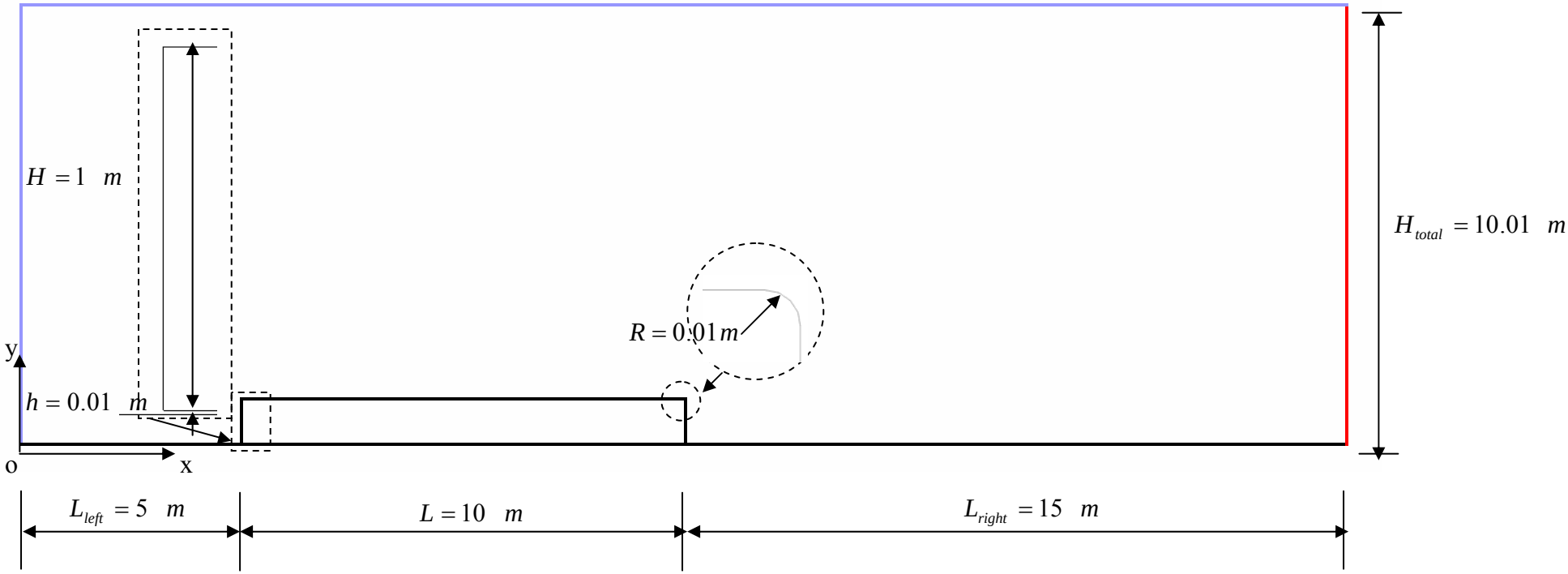

Fig. 6 Geometry for Case 2

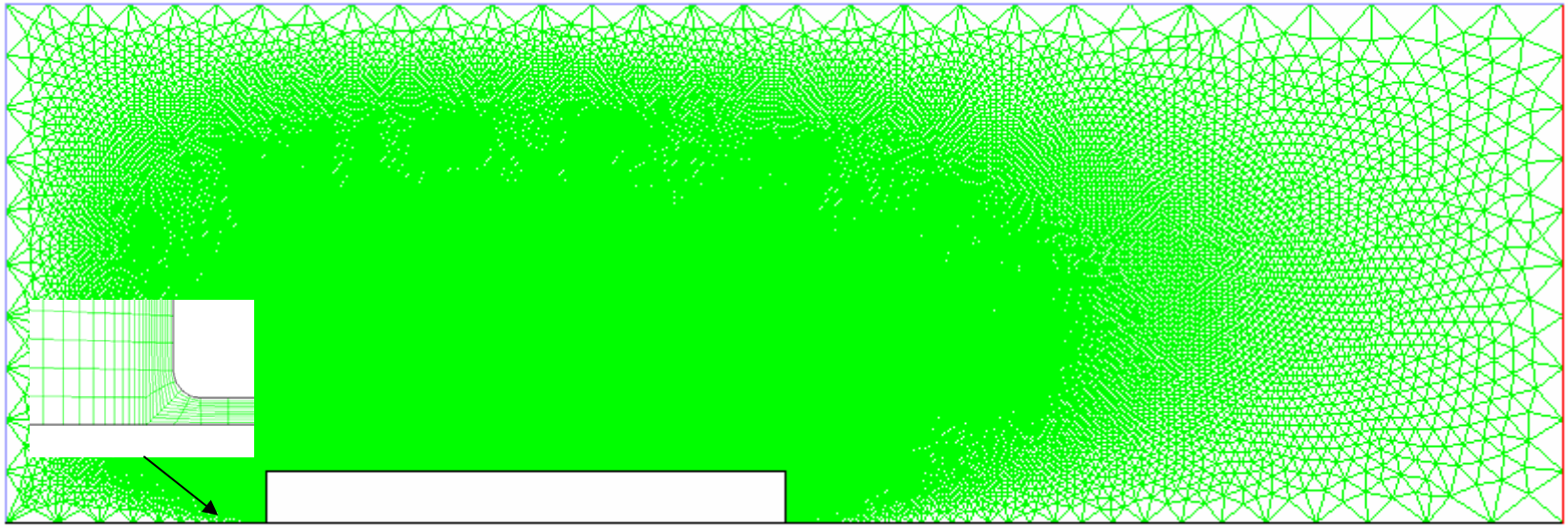

Fig. 7 Mesh for Case 2

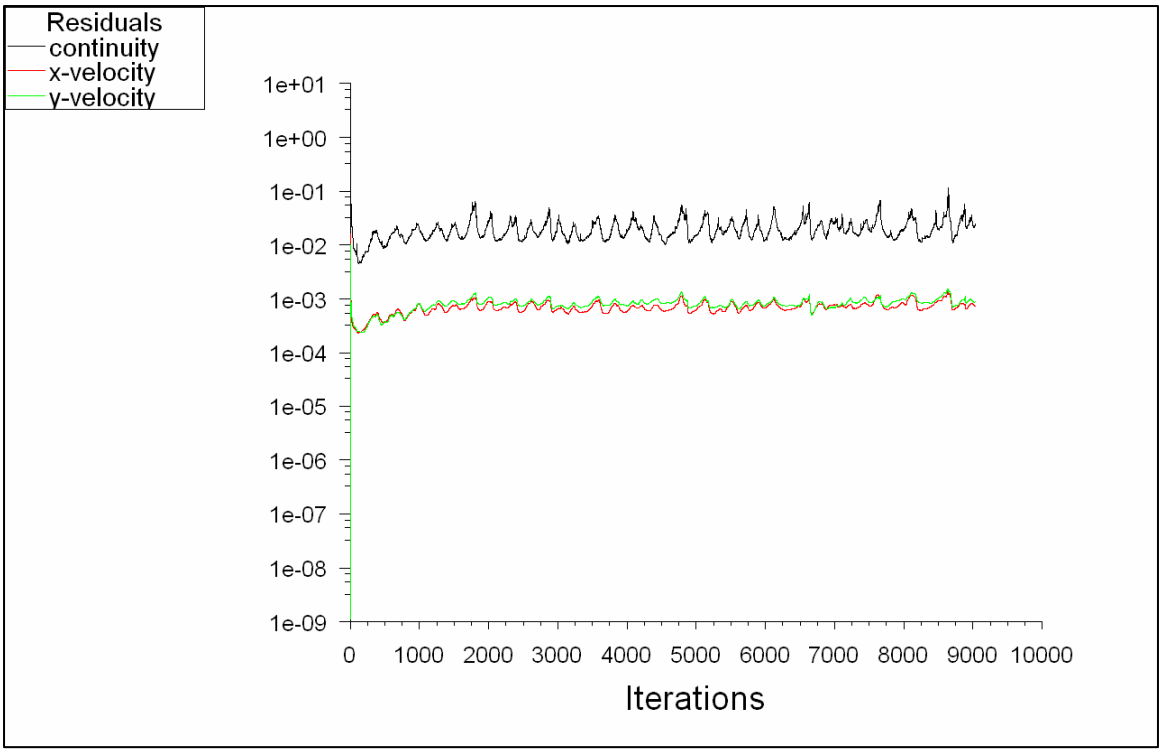

Fig. 8 Scaled residuals for Case 2

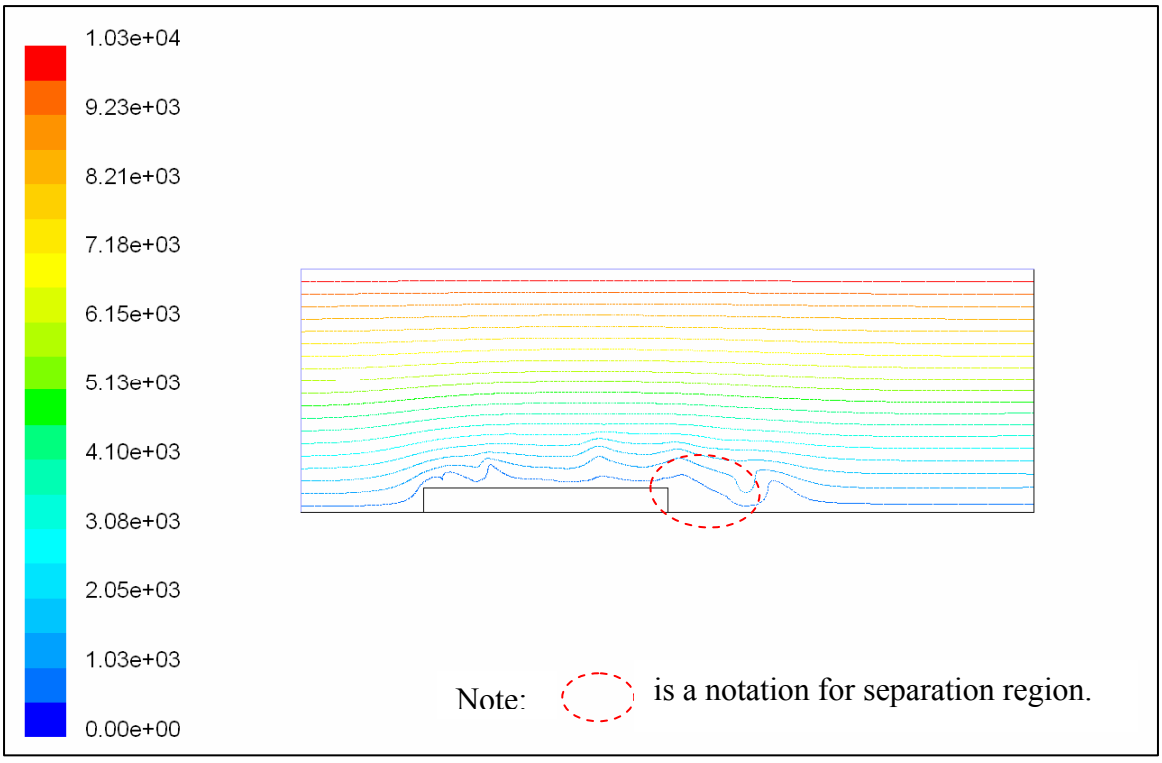

Fig. 9 Contours of stream function (kg/s) for Case 2

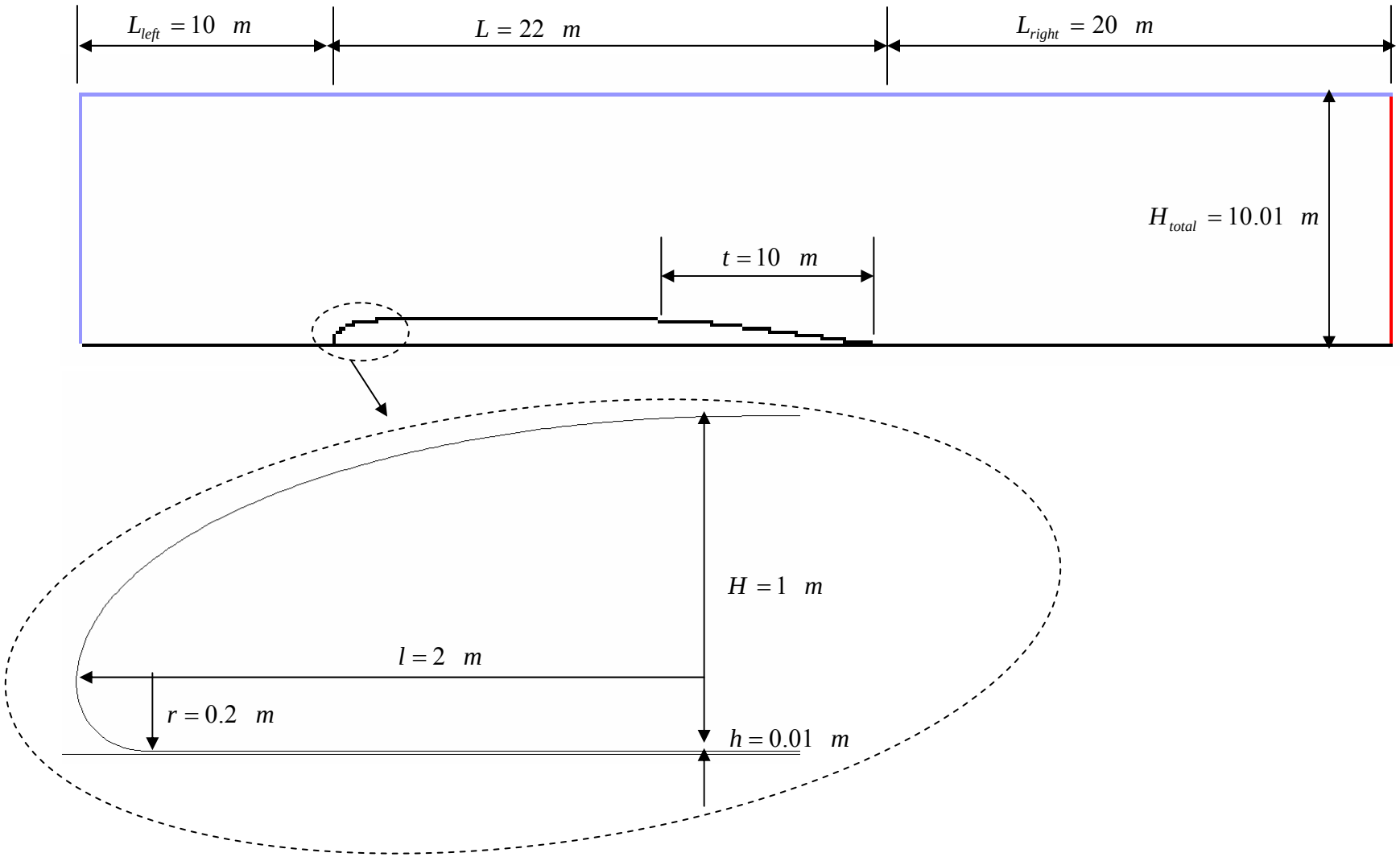

Fig. 10 Geometry for Case 3

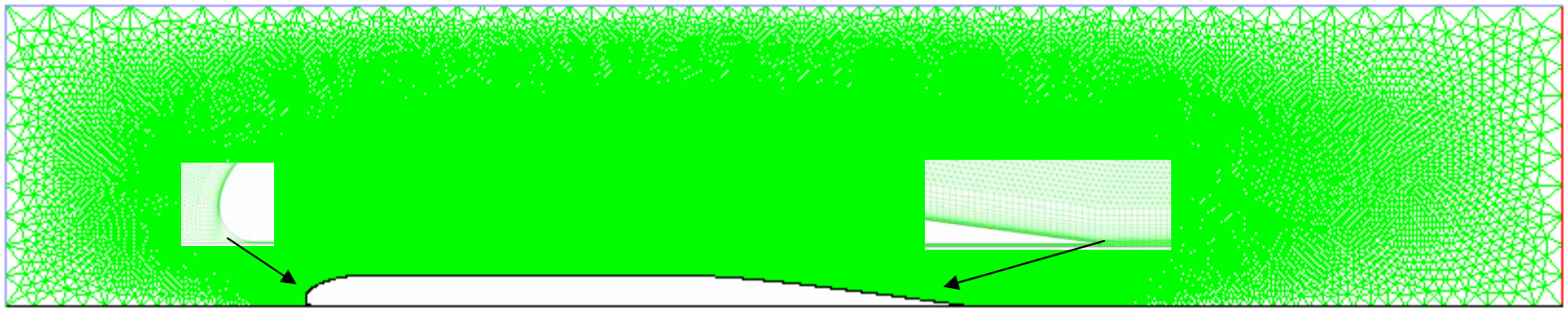

Fig. 11 Mesh for Case 3

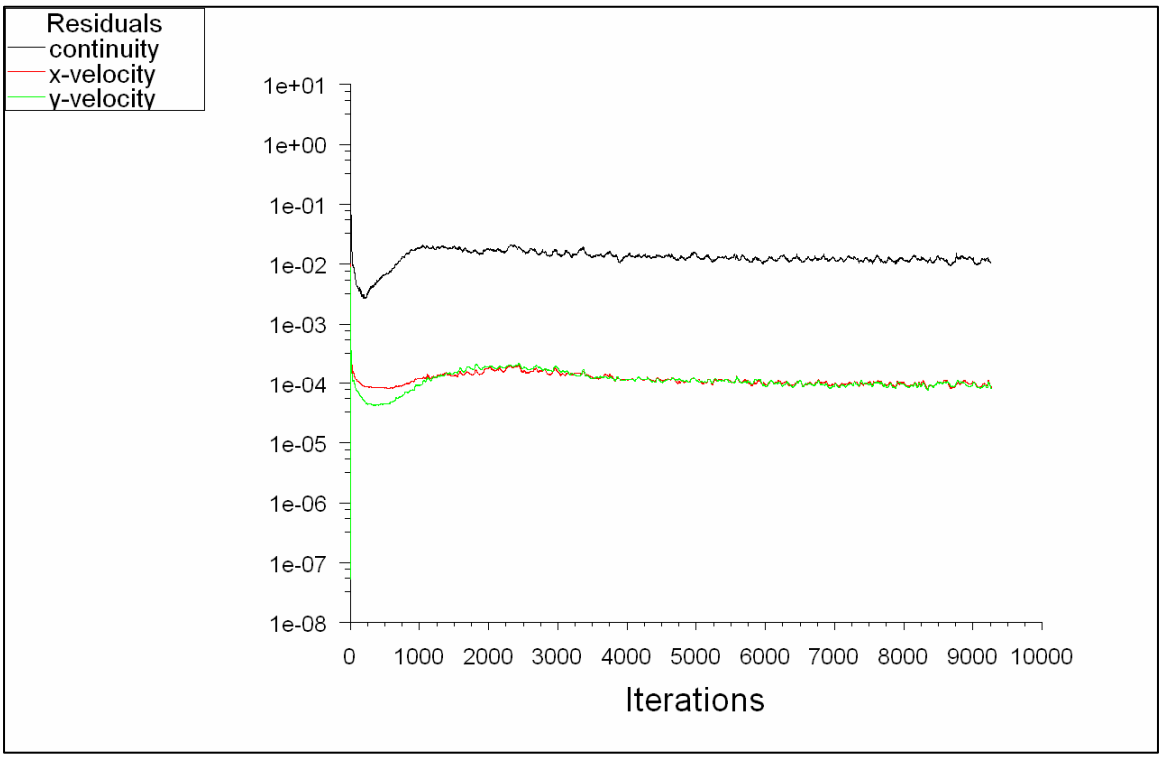

Fig. 12 Scaled residuals for Case 3

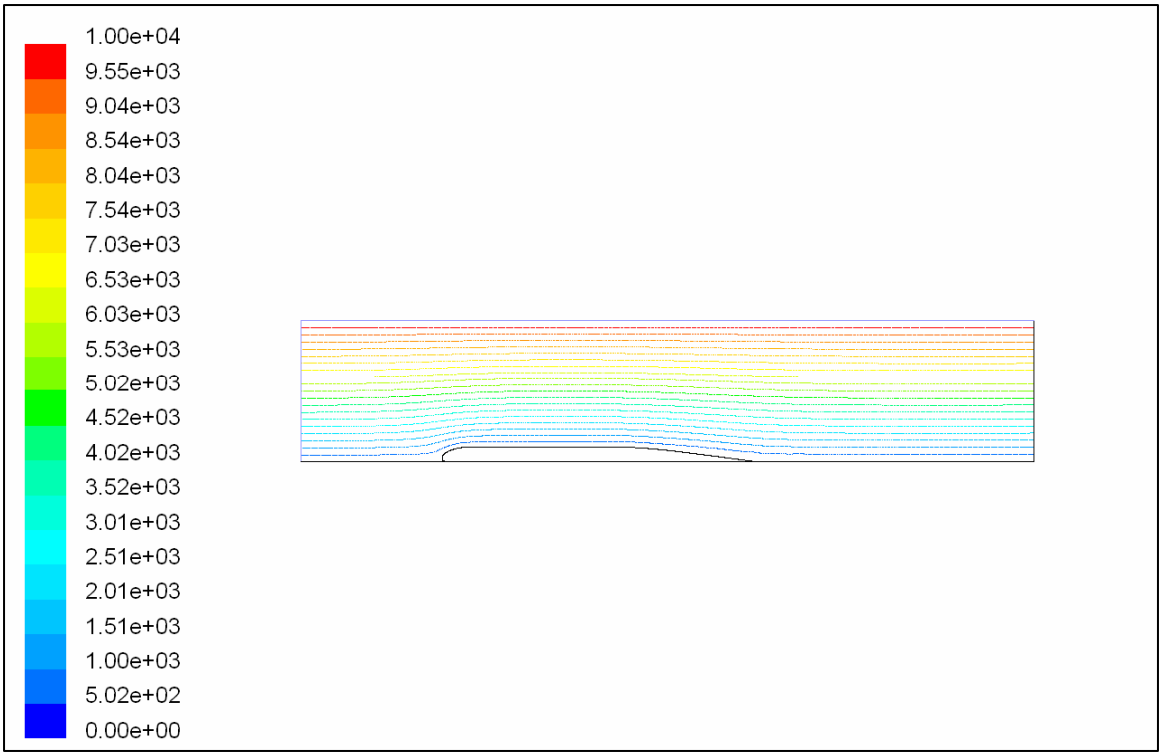

Fig. 13 Contours of stream function (kg/s) for Case 3

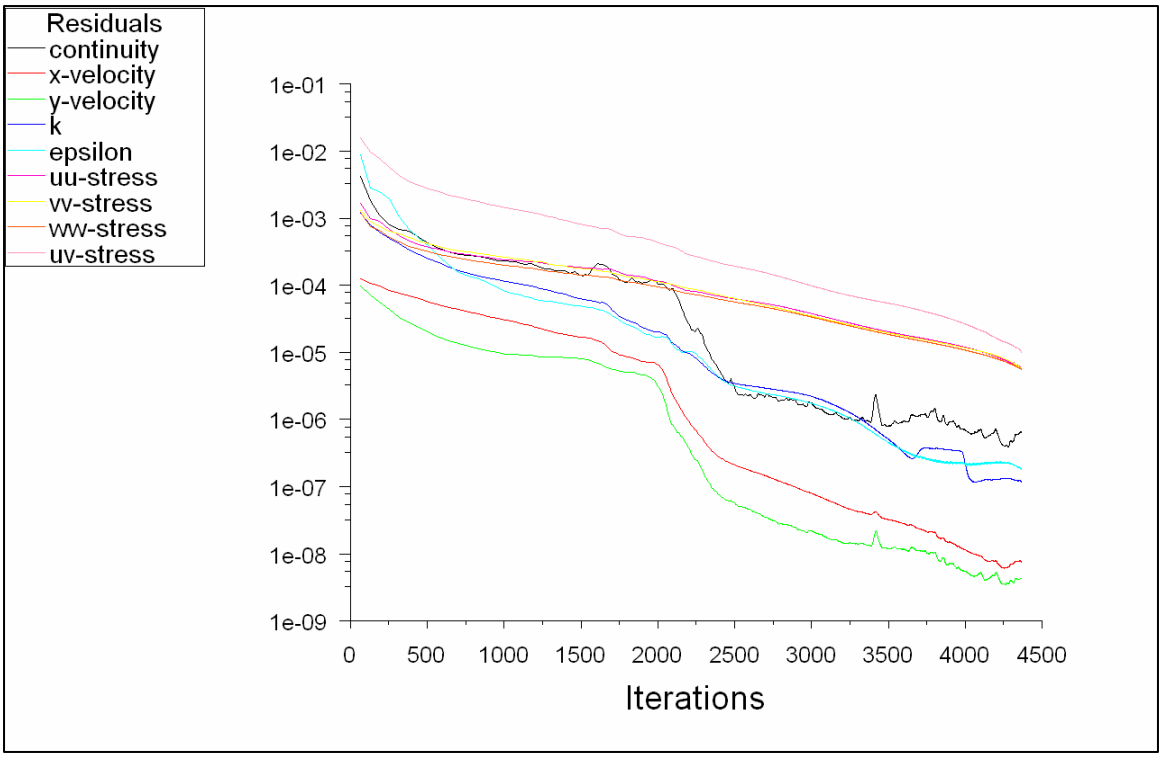

Fig. 14 Scaled residuals for Case 4

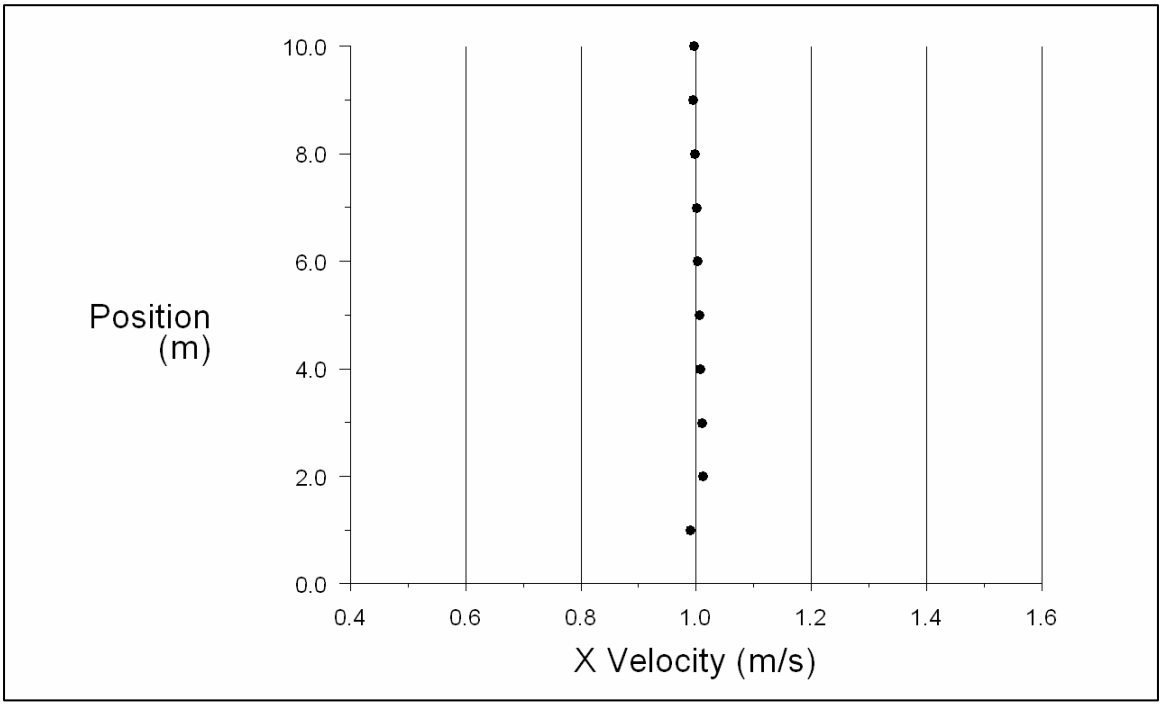

Fig. 15 Horizontal velocity along the right edge for Case 4

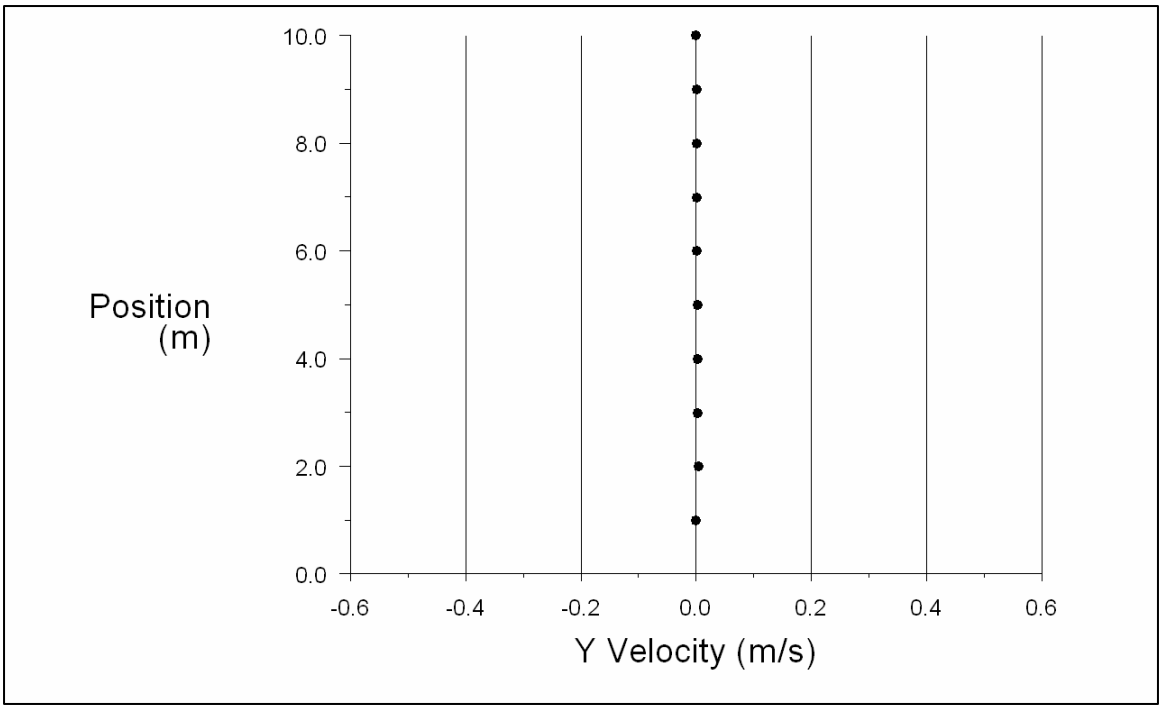

Fig. 16 Vertical velocity along the right edge for Case 4

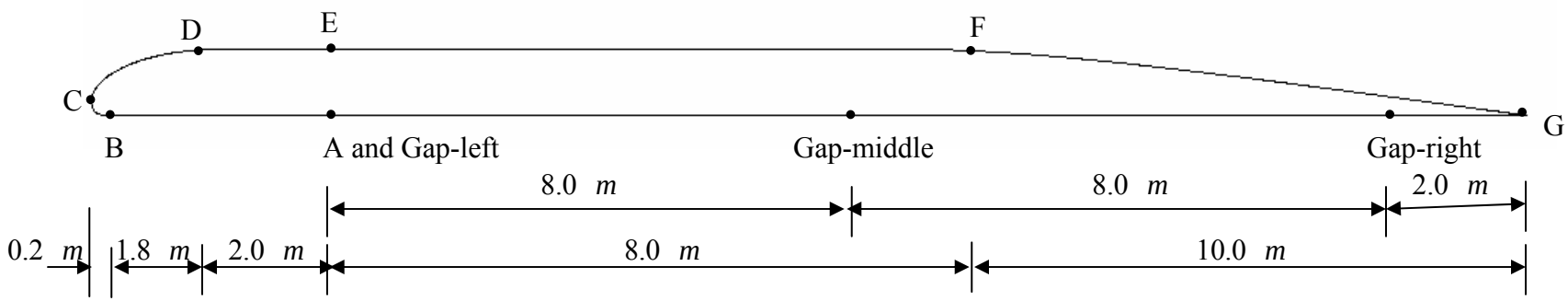

Fig. 17 The four parts of the surface of the soil mass

Fig. 18 Physical & Modeled Flow under Soil Mass

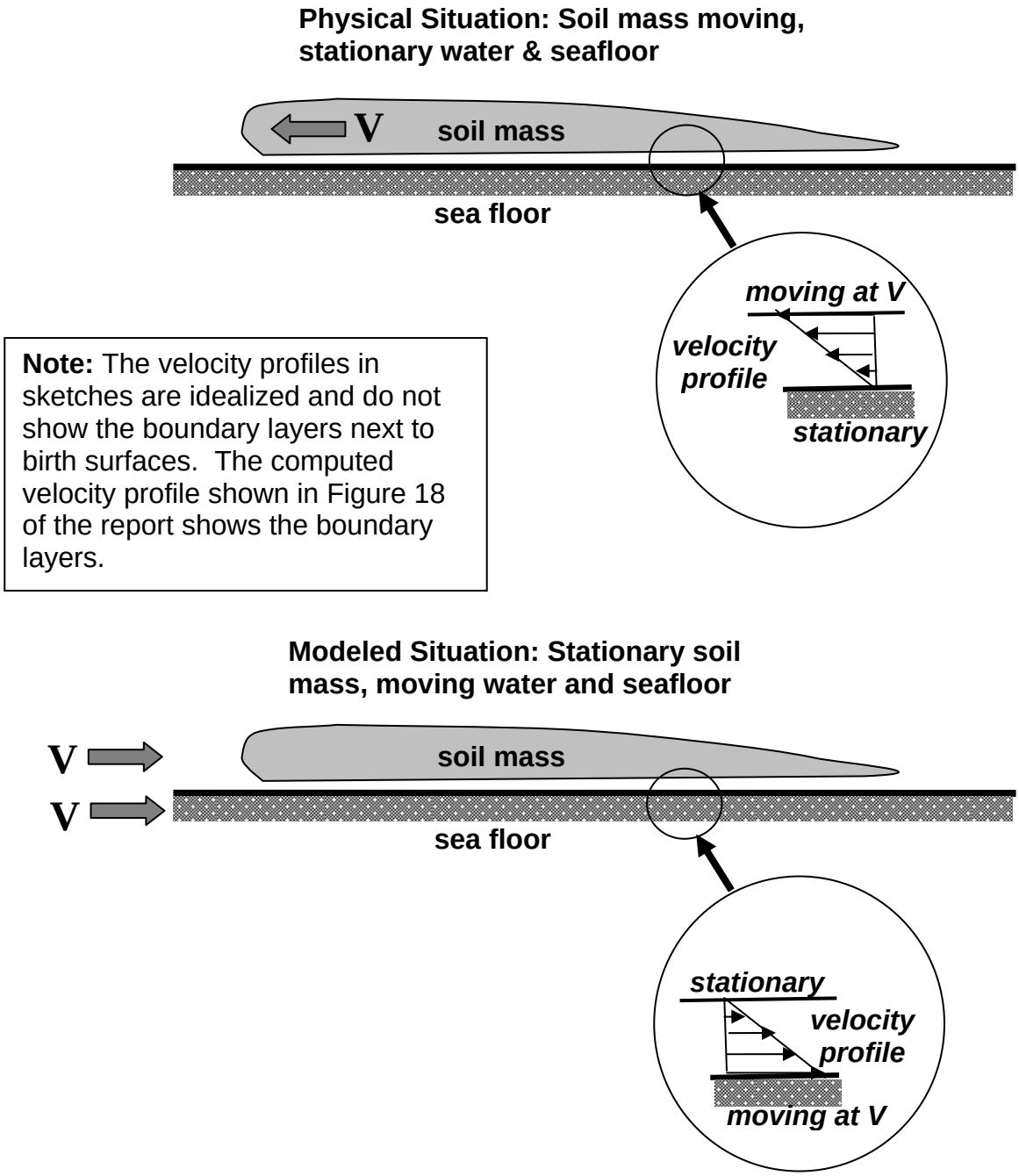

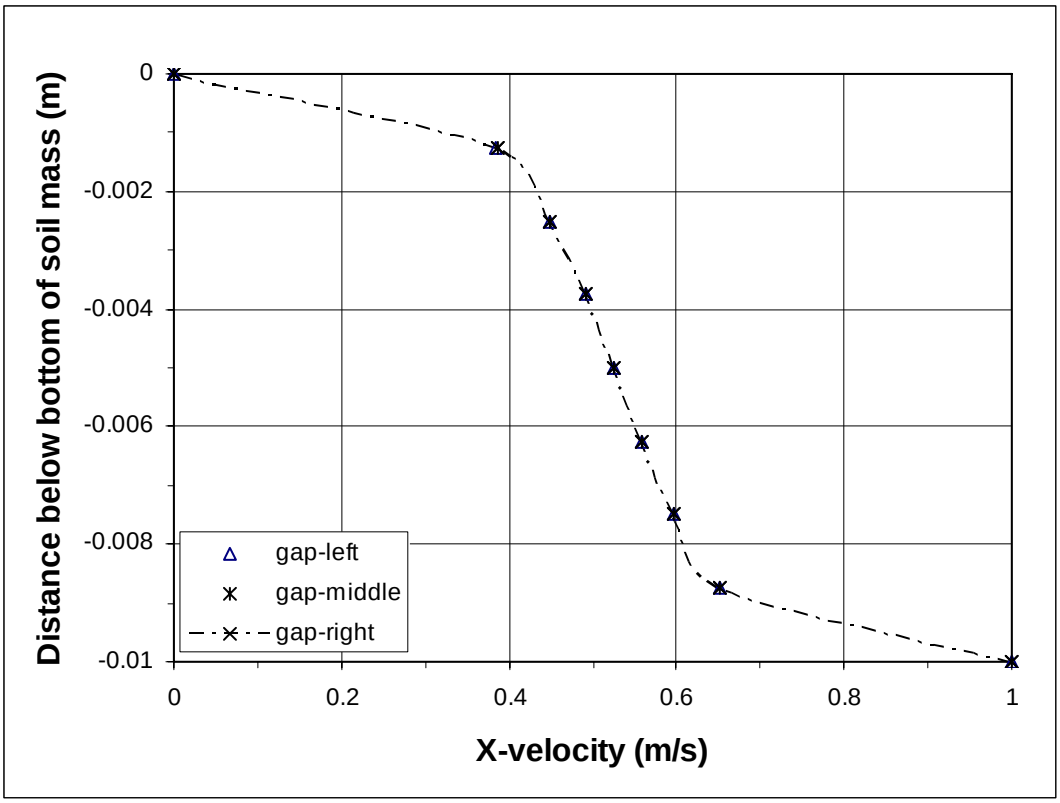

Fig. 19 Horizontal velocity across the gap

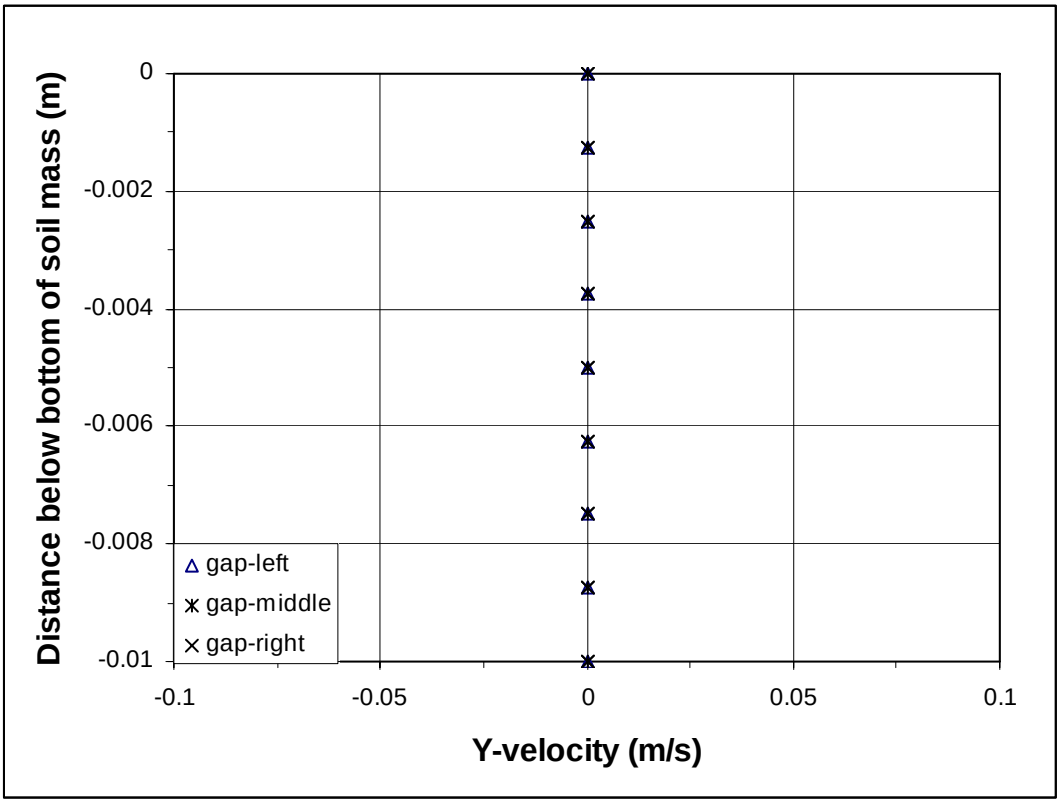

Fig. 20 Vertical velocity across the gap

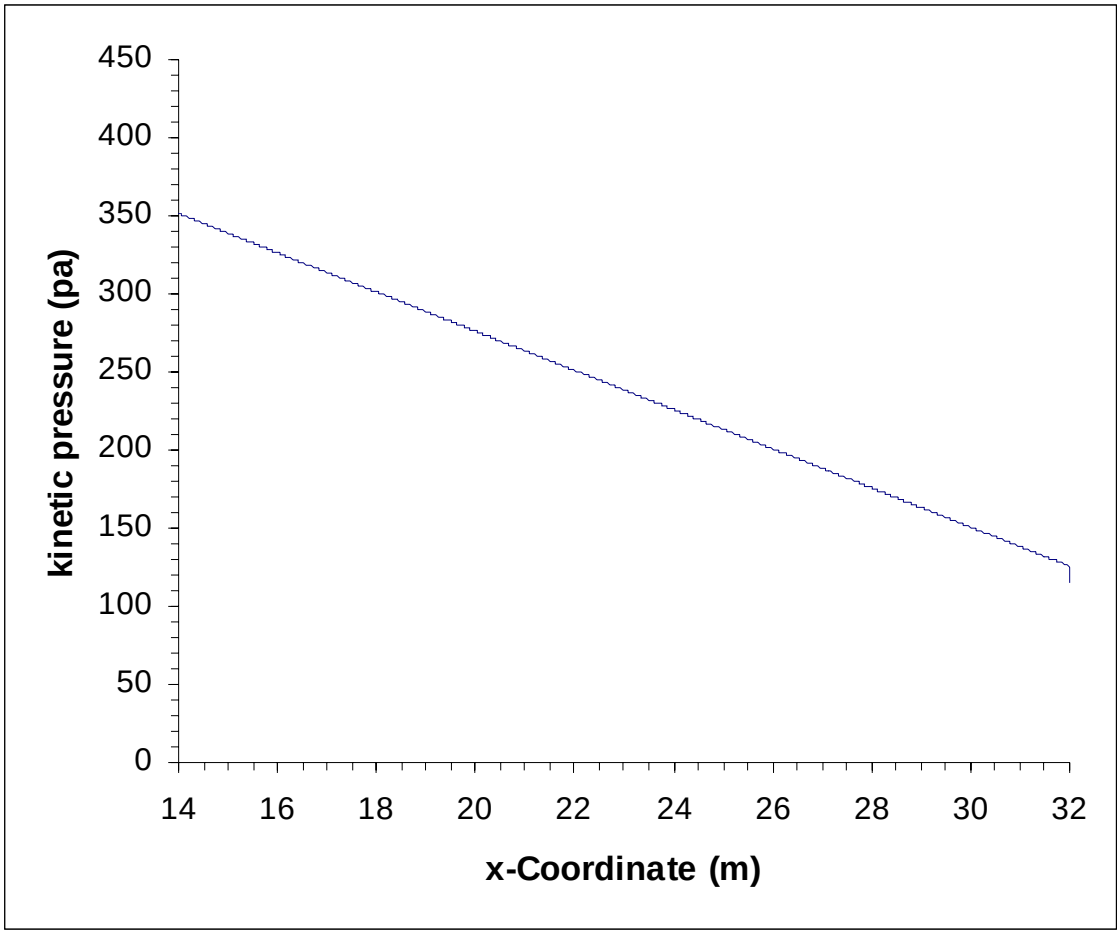

Fig. 21 Kinetic pressure along the bottom of the soil mass

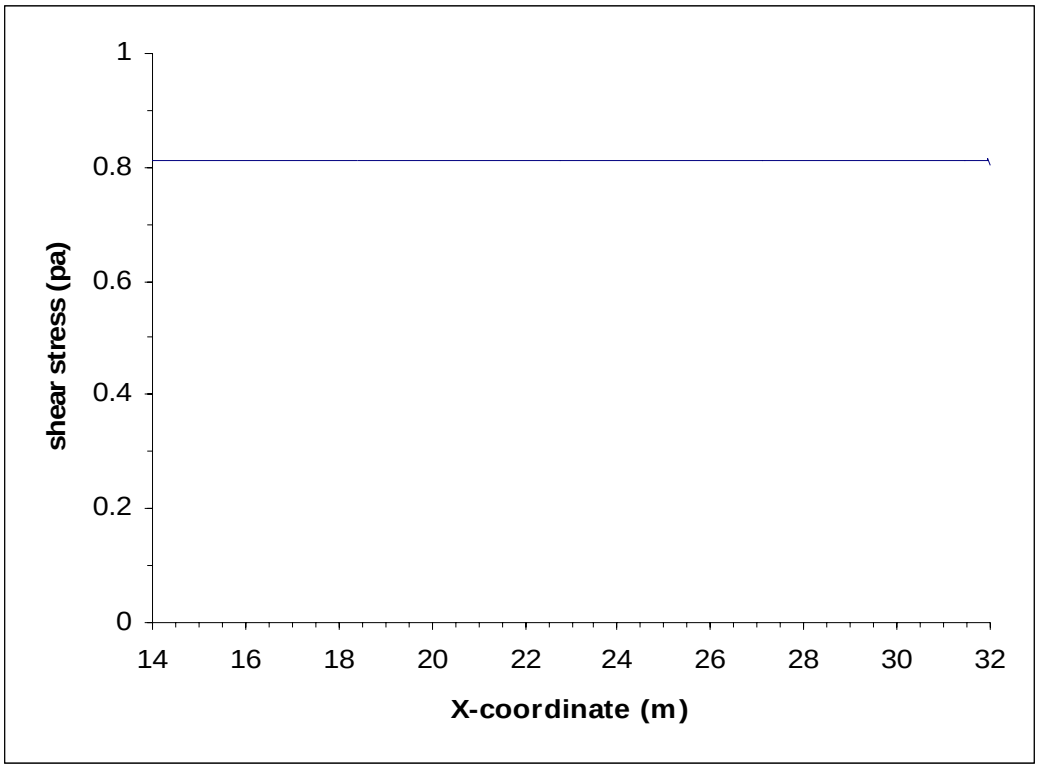

Fig. 22 The distribution of shear stress along the bottom of the sliding mass

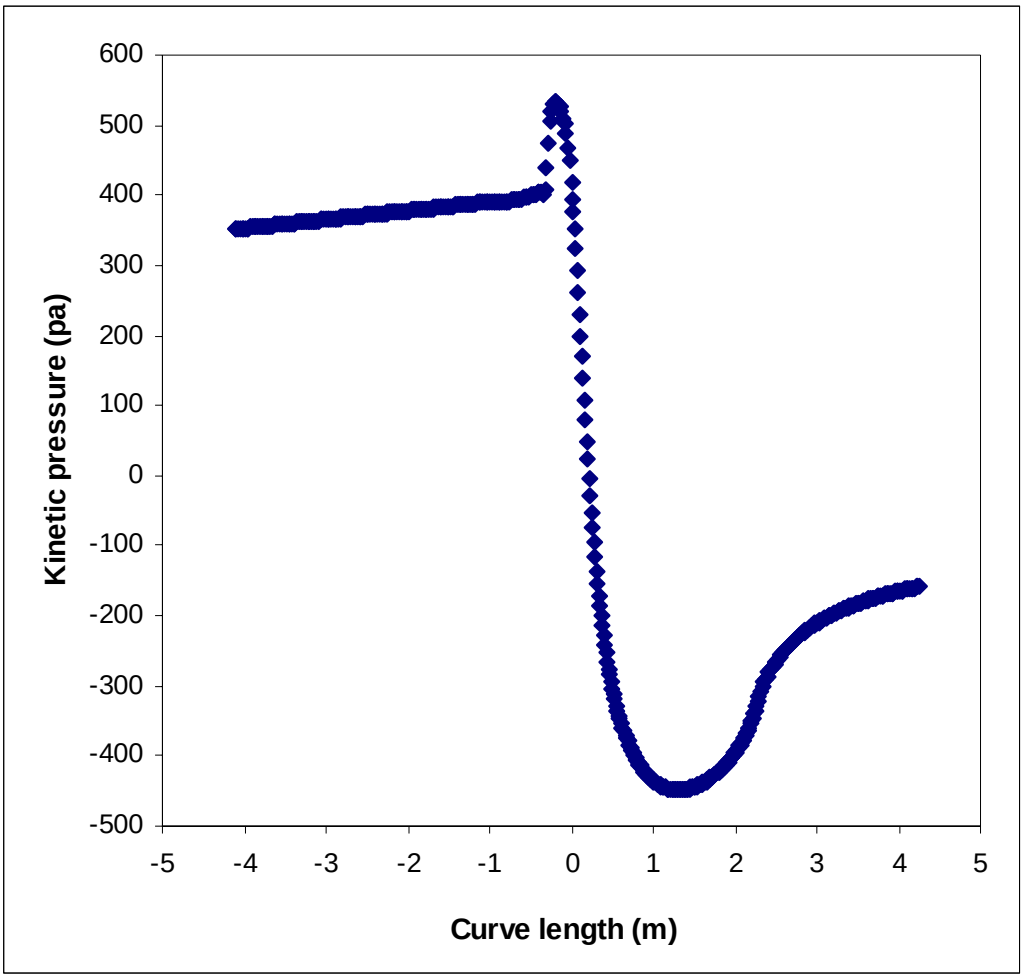

Fig. 23 Pressure distribution around the front of the slide mass

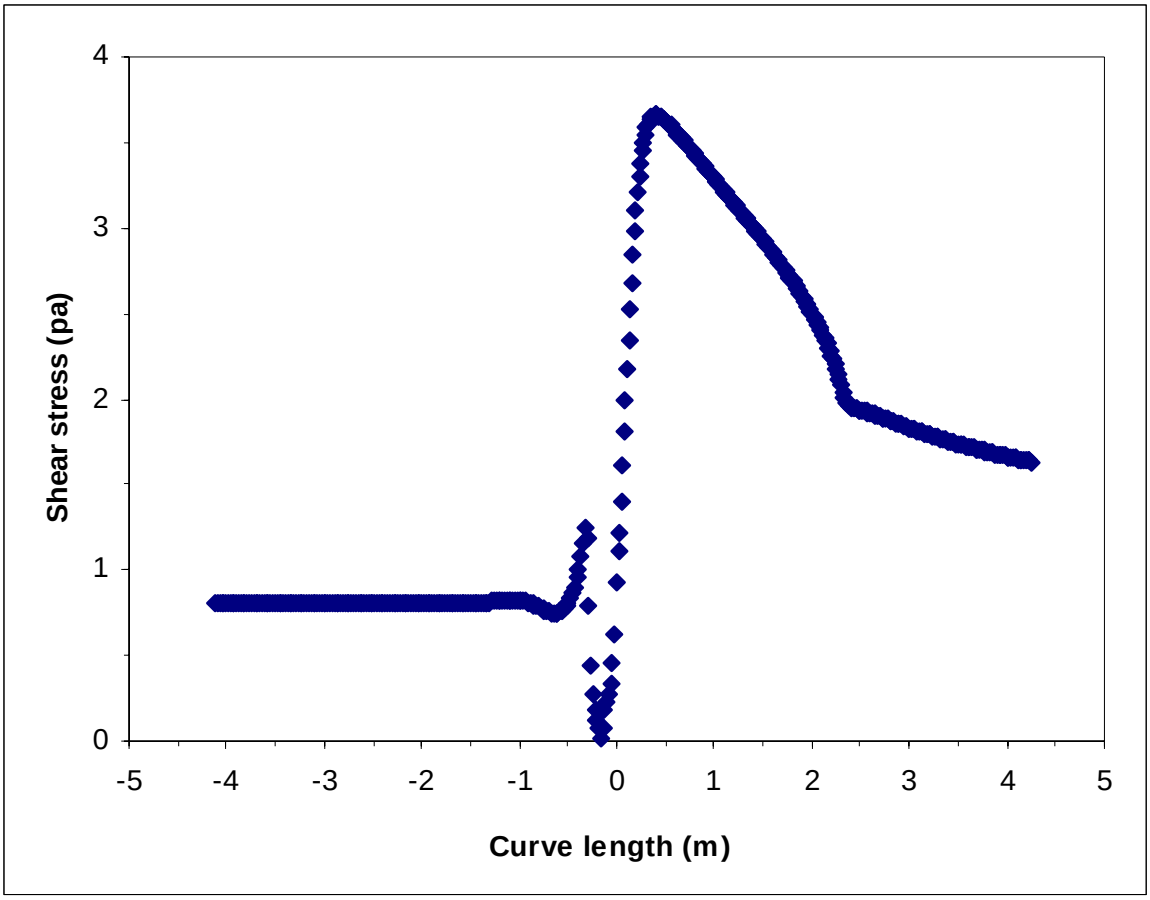

Fig. 24 The distribution of the shear stress around the front of the slide mass

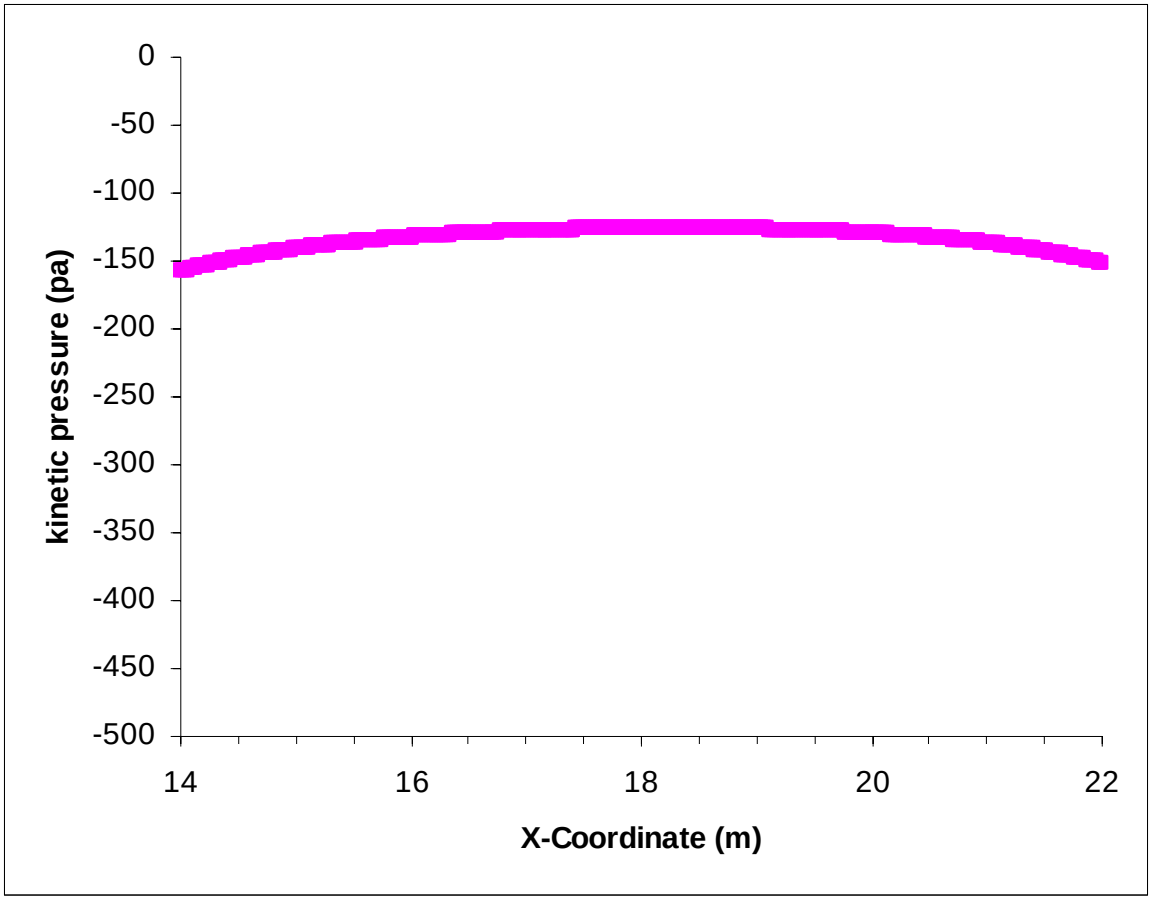

Fig.25 Pressure distribution along the top surface of the soil mass

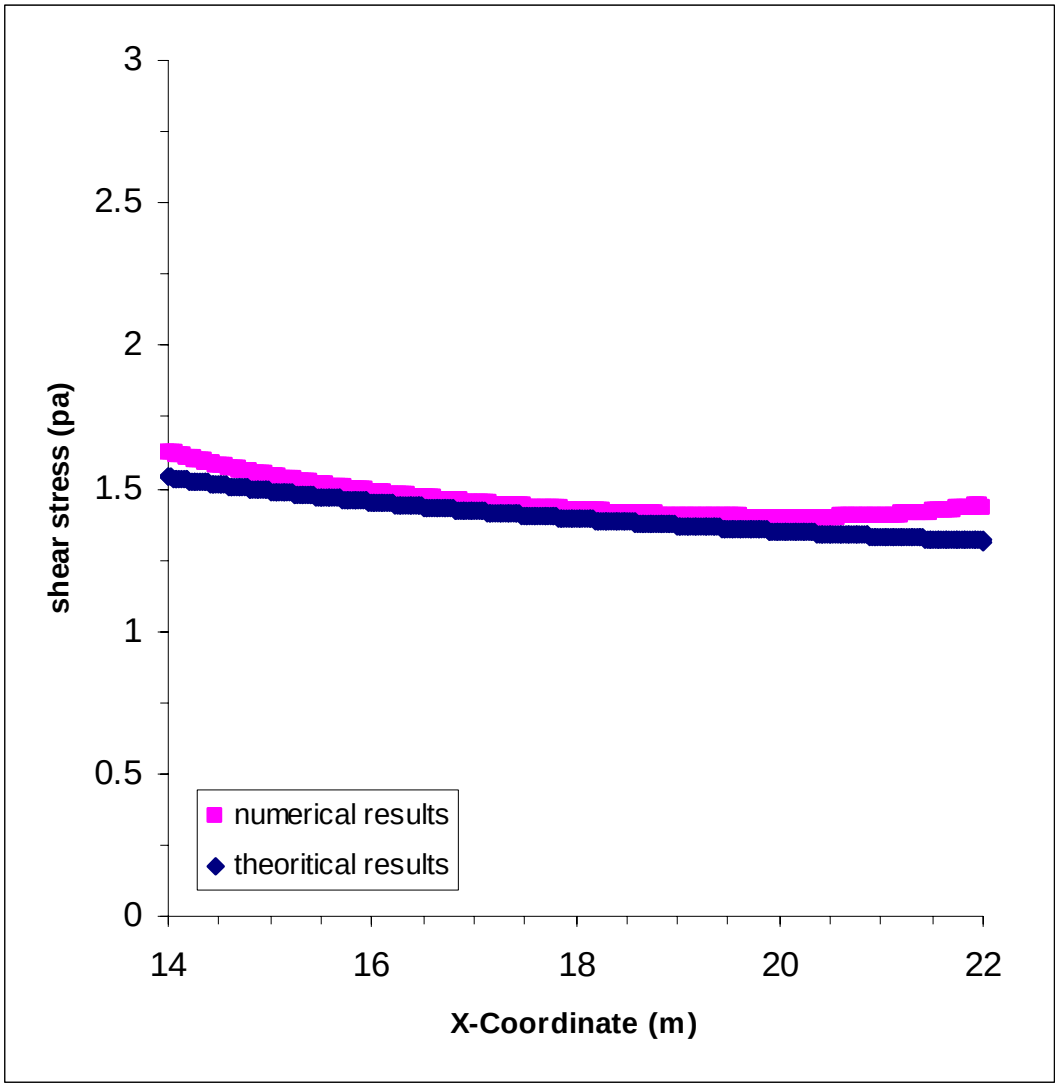

Fig. 26 The distribution of shear stress along the top surface of the soil

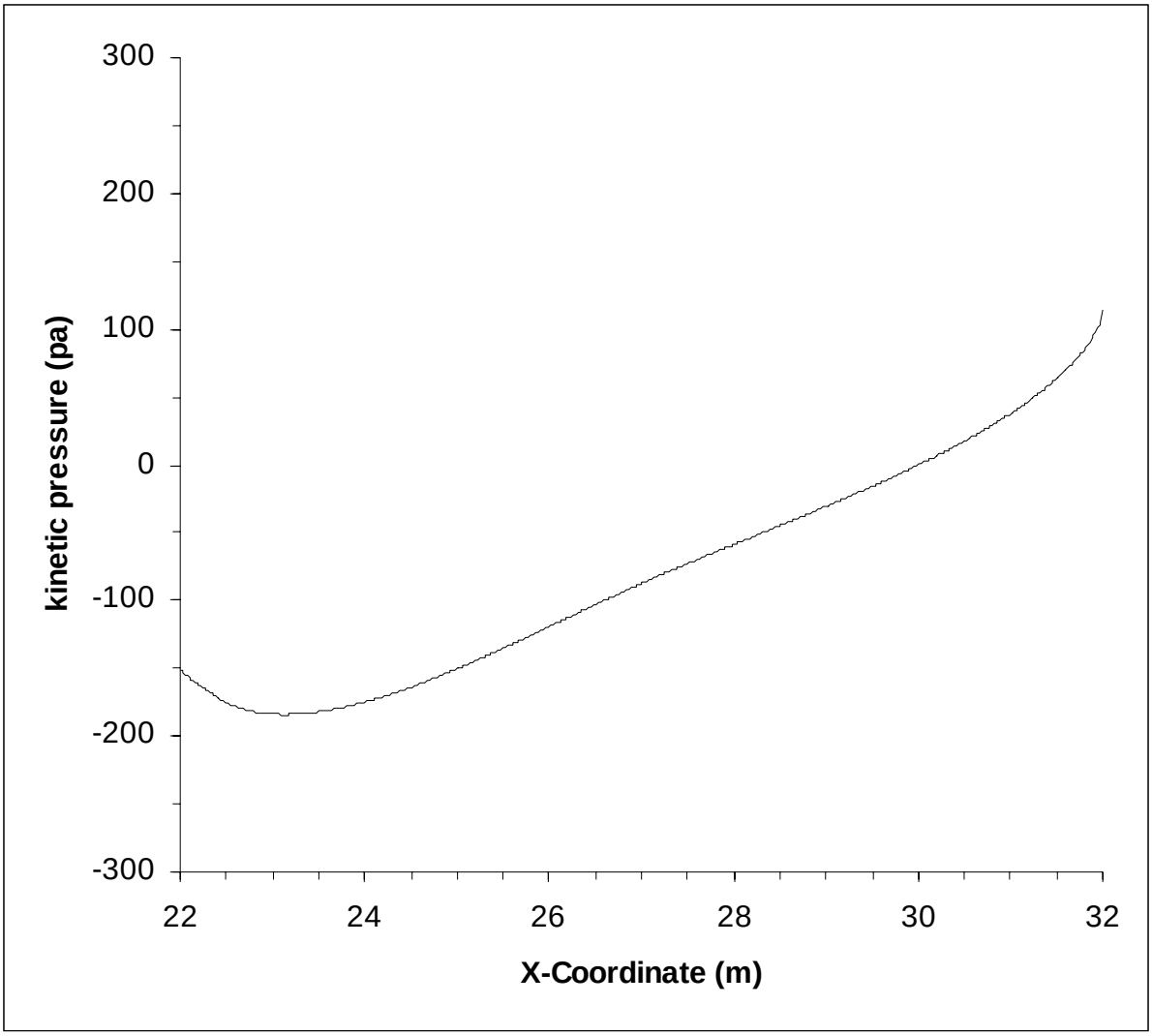

Fig. 27 The distribution of the kinetic pressure on the tail

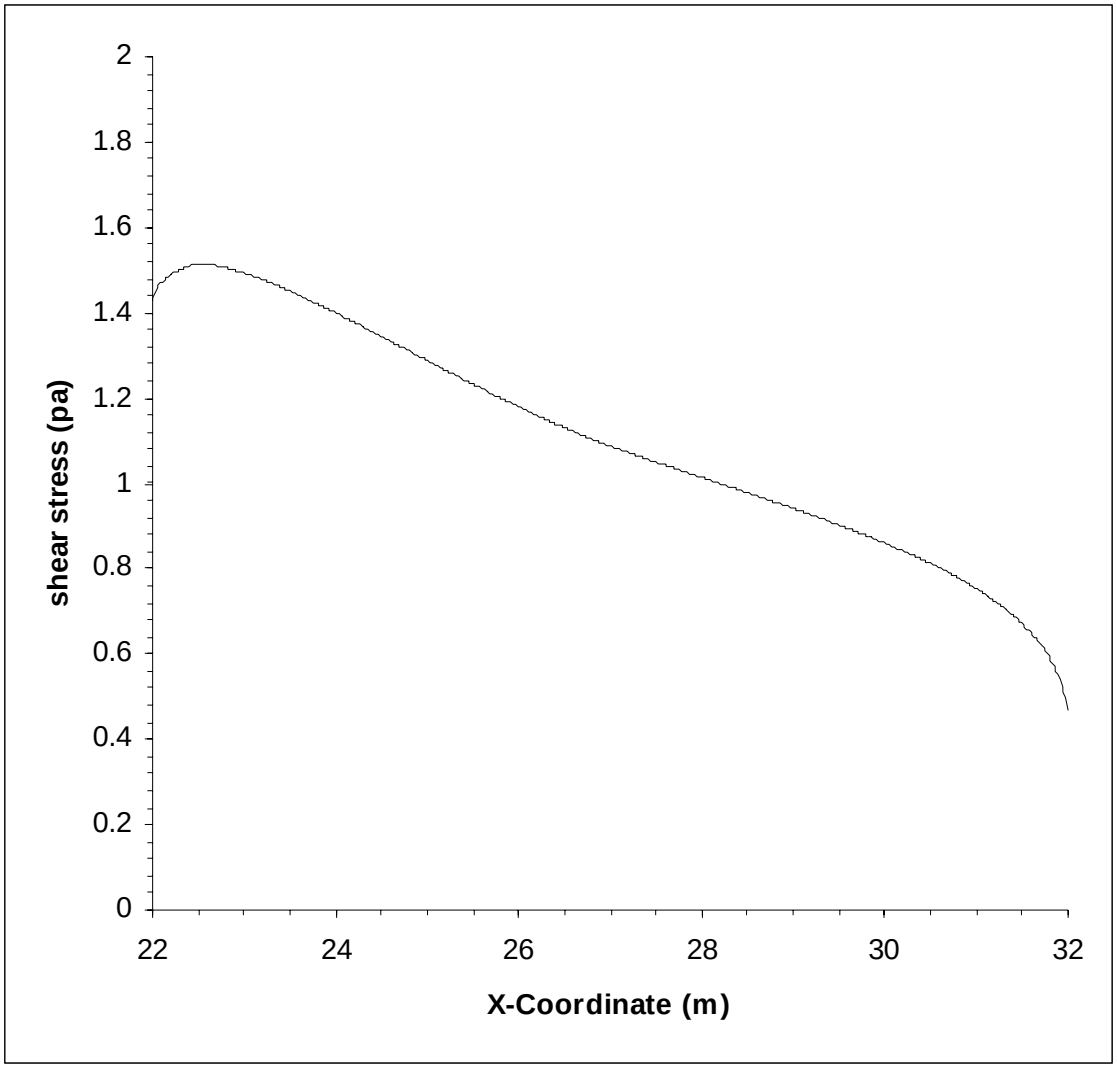

Fig. 28 The distribution of the shear stress on the tail

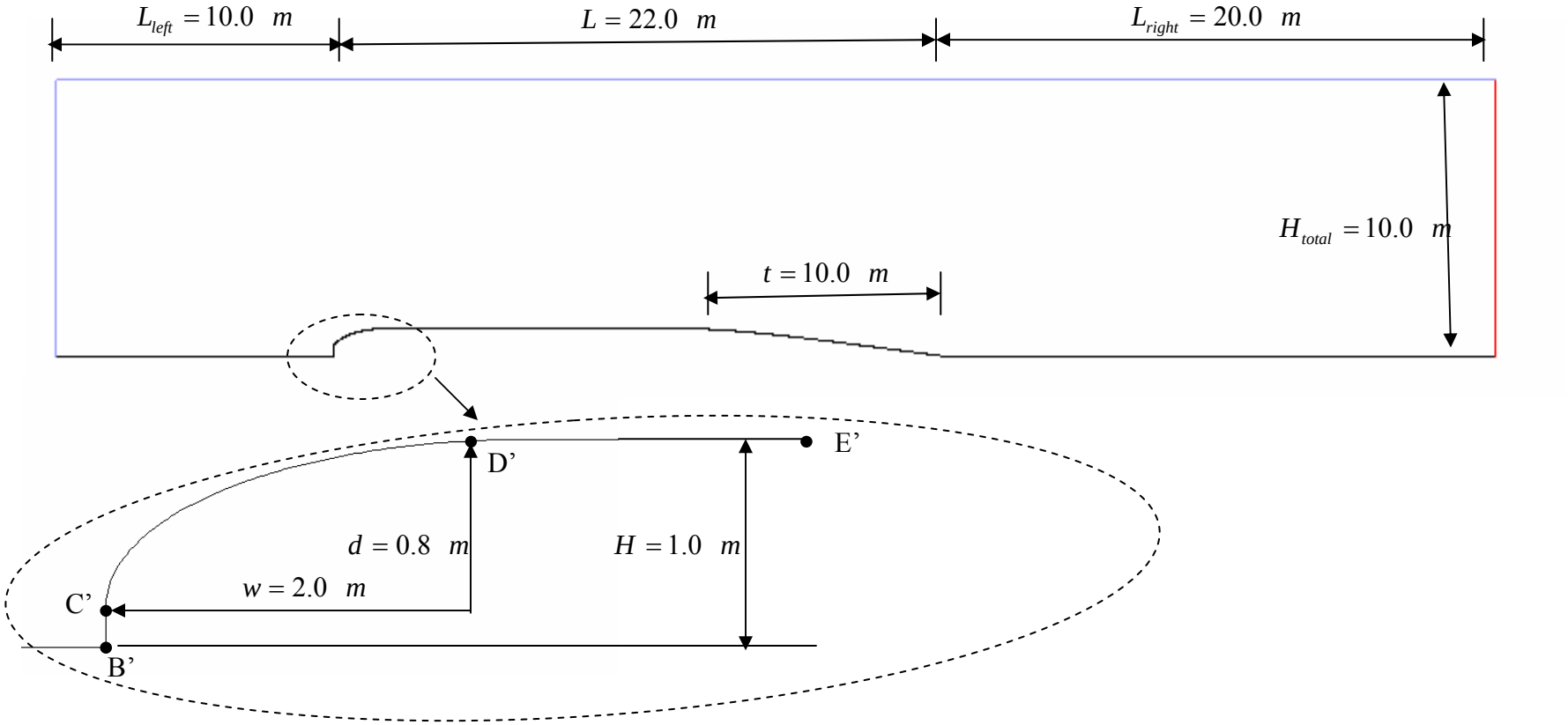

Fig. 29 Geometry for Case 5

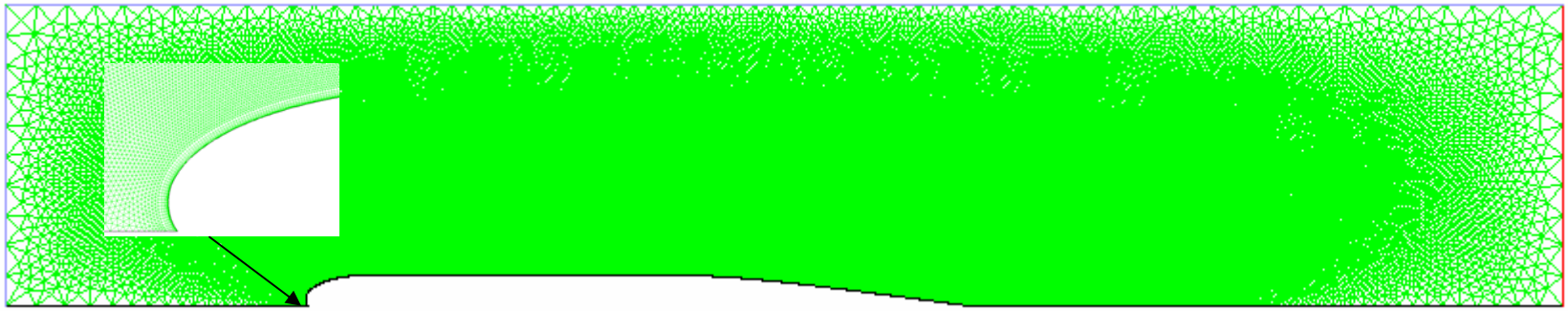

Fig. 30 Mesh for Case 5

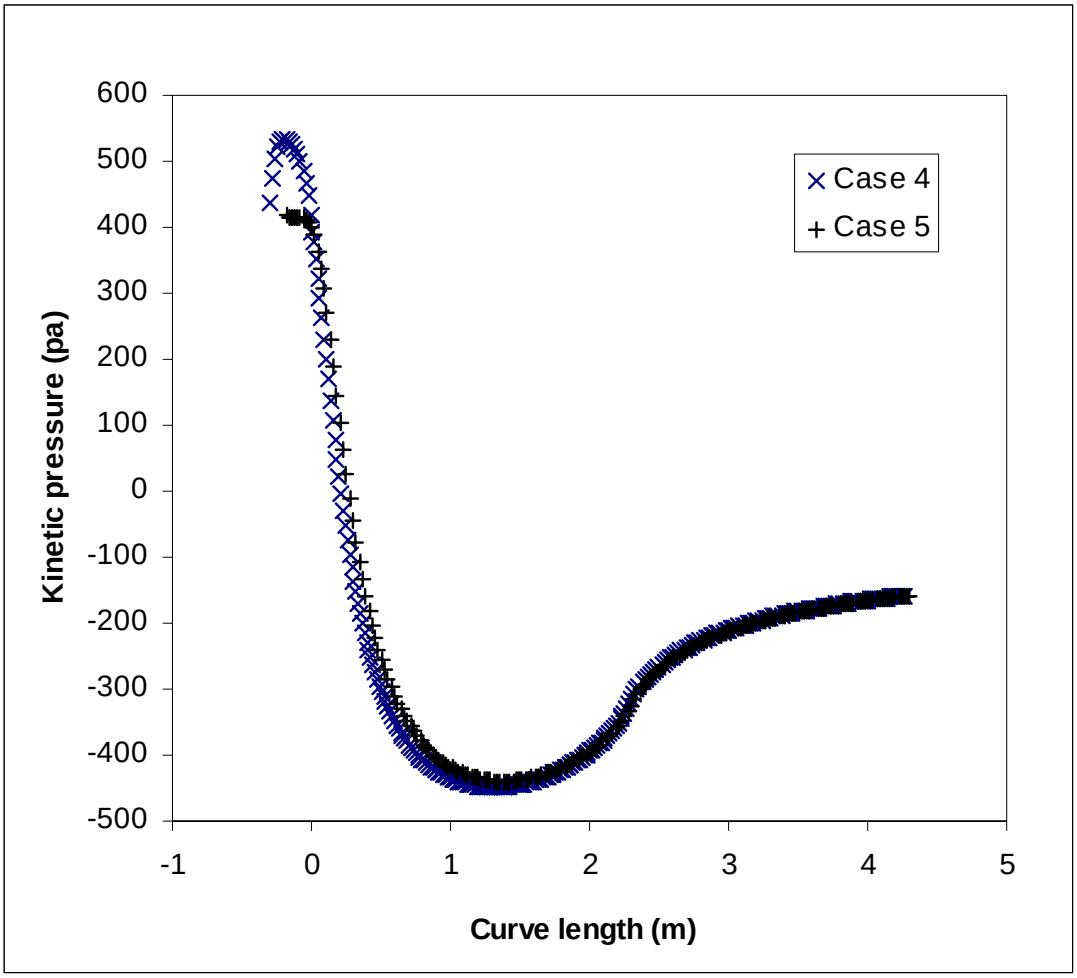

Fig. 31 Pressure distribution around the front of the soil mass for Cases 4 and 5

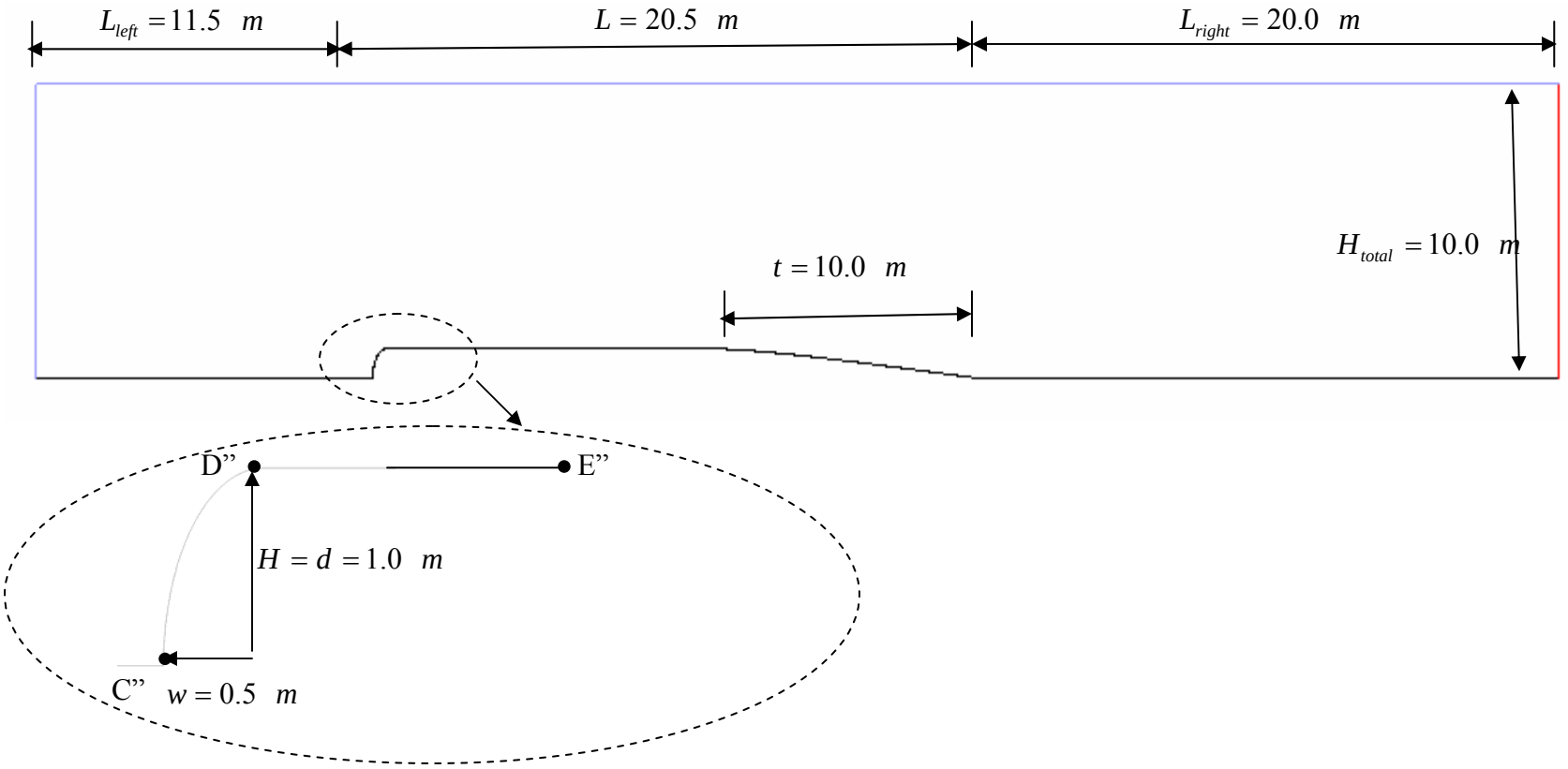

Fig. 32 Geometry for soil mass for Case 6

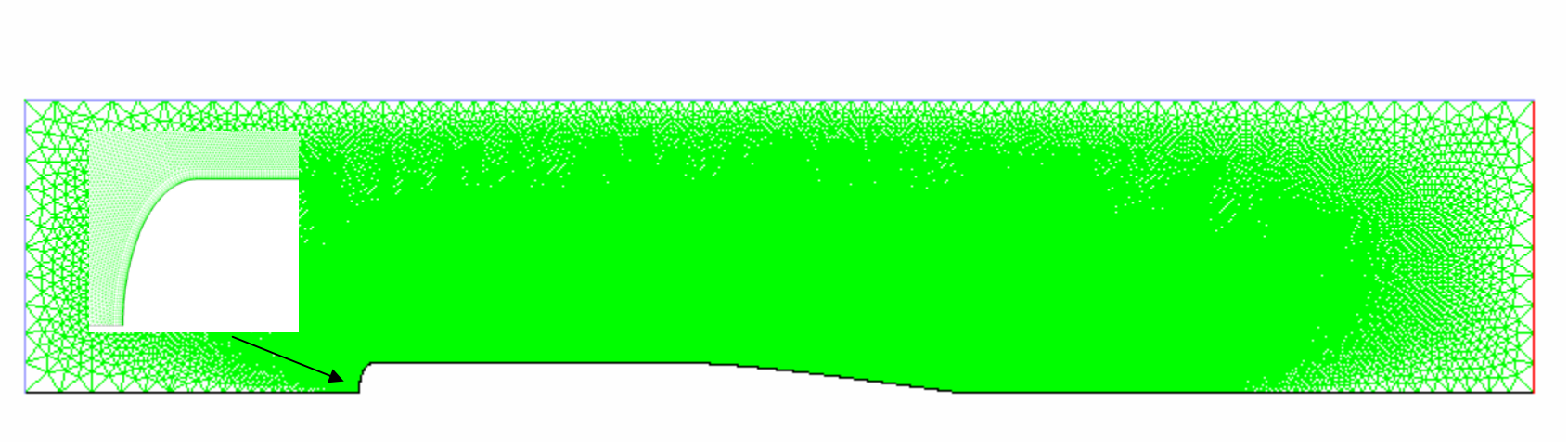

Fig. 33 Mesh for Case 6

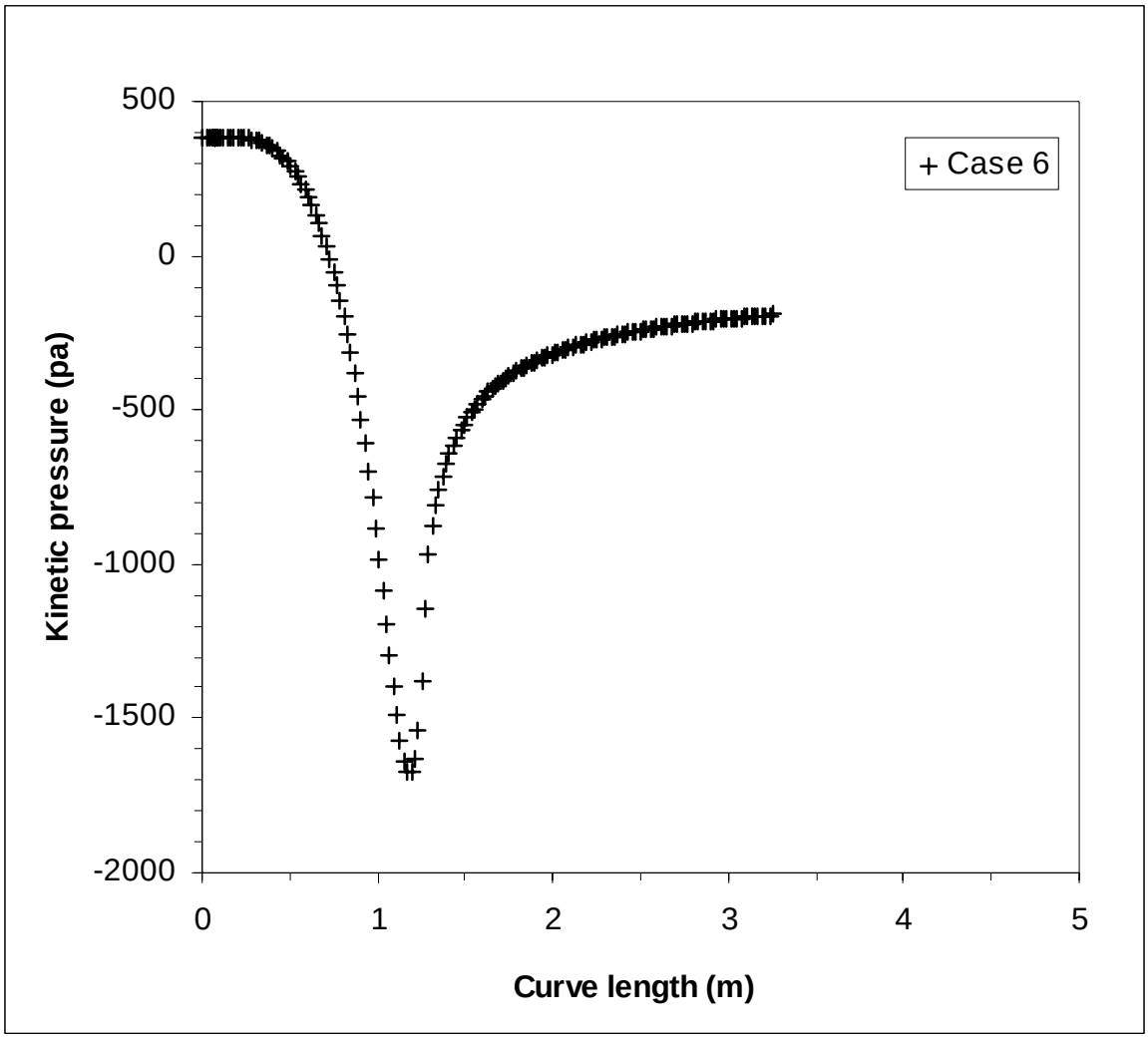

Fig. 34 Pressure distribution around the front of slide mass for Case 6

Table 2: Unit Conversion Chart

Conversion Factors for Different Units of Measurements			
Quantity	**SI Unit**	**Other Unit**	**Inverse Factor**
Length	1m	3.281 feet (ft)	0.3048 m
	1 km	0.540 nautical miles	1.852 km
	1 km	0.6213712 mile	1.609344 km
Area	1 m^2	10.764 ft^2	0.0929m^2
Volume	1 m^3	35.315 ft^3	0.0283 m^3
	1 m^3	264.2 gallon (US)	0.00379 m^3
	1 m^3	220.0 gallon (UK)	0.00455 m^3
	1 m^3	6.29 barrel (US Petroleum)	0.1589 m^3
Velocity	1 m/s	3.281 ft/s	0.305 m/s
	1 m/s	1.943 knot	0.515 m/s
	1 m/s	2.2369 mph	0.44704 m/s
	1 km/hr	0.62137 mph	1.6093 km/hr
Mass	1 kg	2.205 pound	0.454 kg
	1 Mg	0.984 ton (long)	1.016 Mg
	1 Mg	1 tonne (metric)	1 Mg
Force	1 N	0.225 pound force	4.448 N
	1 MN	100.4 ton force	9964 N
	1 MN	224.81 kip	4448 N
	1 kg-force	0.0022046 kip	453.592 kg-force
Pressure	1 N/m^2	0.000145 psi	6895 N/m^2
	1 kg-force/cm^2	0.01422 ksi	70.307 kg-force/cm^2
	1 MN/m^2	20.885 kip/ft^2	47880 N/m^2
Energy	1 J	0.738 foot pounds	1.356 J
Power	1 W	0.00134 horsepower	745.7 W
Temperature	0^0 Celsius	32^0 Fahrenheit	-17.78^0 Celsius
Frequency	1 cycle/s	1 hertz	1 cycle/second
Flow Rates	1 m^3/day	6.289 barrel/day	0.1589 m^3/day
	1 m^3/day	35.3146 ft^3/day	0.0283 m^3/day
Density	1 g/cm^3	0.578 oz./$inch^3$	1.73 g/cm^3